

Characterizing and classifying neuroendocrine neoplasms through microRNA sequencing and data mining

Jina Nanayakkara¹, Kathrin Tyryshkin¹, Xiaojing Yang¹, Justin J.M. Wong¹, Kaitlin Vanderbeck¹, Paula S. Ginter², Theresa Scognamiglio², Yao-Tseng Chen², Nicole Panarelli³, Nai-Kong Cheung⁴, Frederike Dijk⁵, Iddo Z. Ben-Dov⁶, Michelle Kang Kim⁷, Simron Singh⁸, Pavel Morozov⁹, Klaas E.A. Max⁹, Thomas Tuschl⁹ and Neil Renwick^{1,9,*}

¹Laboratory of Translational RNA Biology, Department of Pathology and Molecular Medicine, Queen's University, 88 Stuart Street, Kingston, ON K7L 3N6, Canada, ²Department of Pathology and Laboratory Medicine, Weill Cornell Medicine, 1300 York Avenue, New York, NY 10065, USA, ³Department of Pathology, Albert Einstein College of Medicine, 1300 Morris Park Avenue, Bronx, NY 10461, USA, ⁴Department of Pediatrics, Memorial Sloan Kettering Cancer Center, 1275 York Avenue, New York, NY 10065, USA, ⁵Department of Pathology, Amsterdam University Medical Center, Meibergdreef 9, 1105 AZ Amsterdam, The Netherlands, ⁶Department of Nephrology and Hypertension, Hadassah-Hebrew University Medical Center, Jerusalem 91120, Israel, ⁷Center for Carcinoid and Neuroendocrine Tumors of Mount Sinai, Icahn School of Medicine at Mount Sinai, One Gustave L. Levy Place, New York, NY 10029, USA, ⁸Odette Cancer Center, Sunnybrook Health Sciences Center, Toronto, ON M4N 3M5, Canada and ⁹Laboratory of RNA Molecular Biology, The Rockefeller University, 1230 York Avenue, New York, NY 10065, USA

Received March 06, 2020; Revised May 22, 2020; Editorial Decision May 27, 2020; Accepted June 06, 2020

ABSTRACT

Neuroendocrine neoplasms (NENs) are clinically diverse and incompletely characterized cancers that are challenging to classify. MicroRNAs (miRNAs) are small regulatory RNAs that can be used to classify cancers. Recently, a morphology-based classification framework for evaluating NENs from different anatomical sites was proposed by experts, with the requirement of improved molecular data integration. Here, we compiled 378 miRNA expression profiles to examine NEN classification through comprehensive miRNA profiling and data mining. Following data preprocessing, our final study cohort included 221 NEN and 114 non-NEN samples, representing 15 NEN pathological types and 5 site-matched non-NEN control groups. Unsupervised hierarchical clustering of miRNA expression profiles clearly separated NENs from non-NENs. Comparative analyses showed that miR-375 and miR-7 expression is substantially higher in NEN cases than non-NEN controls. Correlation analyses showed that NENs from diverse anatomical sites have convergent miRNA expression programs, likely reflecting morphological and functional

similarities. Using machine learning approaches, we identified 17 miRNAs to discriminate 15 NEN pathological types and subsequently constructed a multilayer classifier, correctly identifying 217 (98%) of 221 samples and overturning one histological diagnosis. Through our research, we have identified common and type-specific miRNA tissue markers and constructed an accurate miRNA-based classifier, advancing our understanding of NEN diversity.

INTRODUCTION

Classifying neuroendocrine neoplasms (NENs) is challenging due to tumor diversity, inconsistent terminology and piecemeal molecular characterization. Currently, NENs are broadly divided into epithelial or non-epithelial groups based on site of origin and differences in keratin and other gene expression; each group comprises multiple pathological types (1–3). To facilitate comparisons between NENs from different anatomical sites, international experts recently proposed a common classification framework (3). Here, the terms ‘category’, ‘family’, ‘type’ and ‘grade’, respectively, denote predominant neuroendocrine differentiation, degree of differentiation, diagnostic entity and inherent biological activity. While morphological assessment

*To whom correspondence should be addressed. Tel: +1 613 533 6411; Fax: +1 613 533 2907; Email: neil.renwick@queensu.ca

and immunohistochemical staining for chromogranin A, synaptophysin and Ki-67 proteins remain indispensable for confirming neuroendocrine differentiation and assessing tumor grade, other relevant molecular findings will be integrated into this framework over time. These studies will unravel many puzzles in NEN biology, including delineating the molecular differences between well-differentiated neuroendocrine tumors (NETs) and poorly differentiated neuroendocrine carcinomas (NECs) and finding regulatory molecules that underpin the ‘common neuroendocrine multigene program’ (3).

MicroRNAs (miRNAs) are small (19–24 nt) regulatory RNA molecules that can also be used to classify cancer (4,5). miRNAs are highly informative tissue markers because of their abundance, cell-type and disease-stage specificity, and stability in fresh and archived materials (6,7). These molecules also provide valuable mechanistic insights into cellular processes due to computationally predictable interactions with messenger RNAs (mRNAs) (8,9). In addition, miRNA expression profiles can be used to assess data reliability and to prioritize mRNA targets through further organization into miRNA cluster and sequence family datasets (10). To date, multiple miRNA profiling studies have been performed on single or limited combinations of NEN pathological types using different RNA isolation, detection and analysis methods (11). Although these differences complicate interstudy comparisons, miRNAs still hold much promise as multi-analyte markers that better reflect the ‘complexity and multidimensionality of the neoplastic process’ than current mono-analyte markers (12,13). Given recent advances in miRNA detection and analysis (14), we expect that substantial biological and clinically relevant insights into NEN biology will be gained through comprehensive miRNA profiling of multiple pathological types.

Through small RNA sequencing and data mining, we have generated reference miRNA expression profiles for multiple NEN pathological types and site-matched non-NEN controls, identified candidate category- and type-specific miRNAs, found evidence for constitutive and convergent miRNA gene expression in epithelial and non-epithelial NENs, and established a novel multilayer classifier for discriminating NEN pathological types.

MATERIALS AND METHODS

Study design and clinical materials

Sequencing-based miRNA expression profiles from 378 clinical samples, comprising 239 NEN cases and 139 site-matched non-NEN controls, were used in this study. Expression profiles were either compiled from published studies (7,15–18) ($n = 149$) or generated through small RNA sequencing ($n = 229$). Diagnostic histopathology, small RNA cDNA library preparation and the source of each sample are presented in Supplementary Table S1. The use of de-identified clinical data and banked or archived clinical materials was approved through the Research Ethics Board at Queen’s University, the Institutional Review Boards of Memorial Sloan Kettering Cancer Center, The Rockefeller University and Weill Cornell Medicine, and the Medical Ethics Committee at the Amsterdam University Medical Center.

RNA isolation and quantitation

Total RNA was isolated from 306 formalin-fixed paraffin-embedded tissue blocks and 72 fresh-frozen tissue samples using the Qiagen RNeasy[®] Mini Kit ($n = 258$), TRIzol[™] Reagent ($n = 68$), the Ambion RecoverAll[™] Total Nucleic Acid Isolation Kit ($n = 28$), Amsbio RNA-Bee[™] Isolation Reagent ($n = 10$) and Qiagen miRNeasy[®] Mini Kit ($n = 5$), according to the manufacturers’ instructions or as described (7,15–18). Total RNA concentrations were measured using the Qubit[™] fluorometer ($n = 258$), NanoDrop[®] ND-1000 spectrophotometer ($n = 61$) or Agilent 2100 Bioanalyzer ($n = 28$). RNA isolation and quantitation data were unavailable for 9 (2.4%) and 31 (8.2%) samples, respectively.

Small RNA sequencing and sequence annotation

miRNA expression profiles for all 378 samples were generated using an established small RNA sequencing approach and sequence annotation pipeline (10); spiked-in oligonucleotide calibrator markers enabled miRNA quantitation in each sample. Small RNA cDNA libraries were sequenced on HiSeq 2500 Illumina platforms in the Genomics Resource Center, The Rockefeller University, the McGill University and Génome Québec Innovation Center, and the Genomics Core, Albert Einstein College of Medicine. FASTQ sequence files were annotated through an automated pipeline (rnaworld.rockefeller.edu) (10), yielding sequencing statistics and merged miRNA, miRNA cluster and calibrator read counts. Merged miRNA refers to combined counts of multicopy miRNAs from different genomic locations and miRNA clusters are transcriptional units as defined (19); the term ‘miRNA’ will hereafter refer to merged miRNA data. Annotated sequencing statistics for all samples are presented in Supplementary Table S2; miRNA content was calculated using total RNA and calibrator RNA input ratio multiplied by total miRNA and calibrator count ratio as described (7). miRNA, miRNA cluster and calibrator read counts for all samples are presented in Supplementary Tables S3–S5, respectively.

Data preprocessing and filtering

Data preprocessing, filtering and subsequent analyses were performed in MATLAB (Mathworks, Inc., Natick, MA, USA, version R2019a) as described (18). To report miRNA abundance independent of sequencing depth, read counts were normalized against total sequence reads annotated as miRNAs. Sample outliers and batch effects were identified through correlation analyses (20) of miRNA expression profiles and excluded from the final dataset to increase study rigor. These analyses were completed for each NEN pathological type or site-matched non-NEN control group prior to preprocessing of the combined sample set. Sequencing data were of sufficient quality for 221 (92%) of 239 NEN cases and 114 (82%) of 139 non-NEN controls. Most excluded samples were individual outliers, except for 10 non-NEN samples from a single sequencing run. Following preprocessing, all non-human miRNAs and human miRNA STAR sequences were excluded from further analyses. To exclude miRNAs or miRNA clusters with low ex-

pression across samples, a filtering threshold was applied as described (6); specific filtering thresholds were set as a percentile of overall expression as indicated below.

Unsupervised hierarchical clustering of filtered miRNA expression profiles

To assess sample grouping, unsupervised hierarchical clustering was performed using \log_2 transformed normalized read counts of miRNA and miRNA clusters from all preprocessed samples. Euclidean distance was used as the similarity parameter with complete agglomeration clustering applied in the heatmap.2 function of the R gplots package (www.rdocumentation.org/packages/gplots/versions/3.0.1.1). Lowly expressed miRNAs and miRNA clusters were excluded with the filtering threshold set as the top 75% abundant miRNA and clusters in at least one sample.

Assessment and comparative analyses of abundant miRNAs in NEN and non-NEN samples

To identify candidate miRNA markers for all NENs and for each NEN pathological type, we ranked miRNAs and miRNA clusters by abundance and considered the top 1%. These abundant miRNAs and miRNA clusters were compared and correlated between NEN cases and non-NEN controls, as well as between each pathological type and site-matched non-NEN control group. To highlight substantial differences in miRNA expression, only comparisons with 20-fold or greater difference are discussed. For single-member miRNA clusters, abundance measures approximate the abundance of the single miRNA, and are not separately discussed.

Discovery analyses for miRNA-based NEN classification

To identify miRNAs or miRNA clusters that accurately discriminate between or within epithelial or non-epithelial NENs, we used an established feature selection algorithm that is an ensemble of 12 different machine learning techniques with 5-fold cross-validation (20). To prioritize high expression, we set the filtering threshold to the 90th percentile; miRNAs or miRNA clusters expressed above this threshold in >5% of samples were retained. Next, we ranked miRNAs and miRNA clusters that discriminate epithelial from non-epithelial NENs (comparison A). We subsequently ranked miRNA markers that successively identified epithelial NENs, including parathyroid adenoma (PTA), pituitary adenoma (PitNET), Merkel cell carcinoma (MCC), medullary thyroid carcinoma (MTC) and lung NENs from gastrointestinal–pancreatic (GEP) NENs (comparisons B–F), respectively. Lastly, we identified miRNA markers that discriminated neuroblastoma (NB), pheochromocytoma (PCC) and extra-adrenal paraganglioma (PGL) from each other (comparisons G and H) within the non-epithelial group. Only the top-ranking 3% miRNAs and miRNA clusters in these comparisons were assessed for classification below.

Construction and cross-validation of multilayer classifier

Scaling our existing approach to miRNA-based NEN classification (18,20), we constructed and cross-validated a mul-

tilayer classifier for discriminating NEN pathological types based on selected miRNAs. For each decision layer, all available algorithms ($n = 23$) in the MATLAB Classification Learner App were evaluated using 5-fold cross-validation. In each case, the classification model with highest accuracy was a support vector machine (SVM) classifier that was used to identify the smallest subset of miRNAs with the most discriminatory power for comparisons A–H above. Based on these subsets, we constructed a multilayer classifier through which miRNA profiles were first assigned as epithelial or non-epithelial prior to assignment to a specific pathological type.

Assessment of classifier performance and transferability

To assess the performance and transferability of our multilayer classifier, we used t-stochastic neighbor embedding (t-SNE) to visualize sample grouping patterns based on miRNAs selected for classification. We also determined overall classifier accuracy, evaluated the impact of miRNA cluster member substitutions on classifier accuracy and inspected the expression levels of the selected miRNAs.

Statistical analyses

Statistical analyses of clinical parameters were performed using SPSS Statistics (IBM, Armonk, NY, USA, version 25) and MATLAB. Differences in miRNA content and normalized miRNA expression were evaluated between NEN and non-NEN samples, and within NEN pathological types using the non-parametric Kruskal–Wallis (K–W) test (21); a two-sided P -value of <0.05 was considered significant. Similarities in miRNA expression between samples were determined using Spearman's correlation (22).

RESULTS

Anatomical distribution and histopathological diagnoses of study samples

To characterize and compare miRNA expression between NEN and non-NEN samples, we collected relevant study materials, generated comprehensive miRNA expression profiles through barcoded small RNA sequencing, quality controlled profiles through data preprocessing and performed downstream analyses using statistical and machine learning approaches. Following data preprocessing for quality control, our final study cohort comprised 221 NEN cases and 114 site-matched non-NEN controls, hereafter termed study samples (Table 1). NEN cases comprised 15 distinct pathological types, arising in seven anatomical sites, including the gastrointestinal tract and pancreas, lung, parathyroid gland, pituitary gland, skin, thyroid gland, and the adrenal gland and extra-adrenal sites. Site-matched non-NEN controls comprised non-diseased tissues and non-NEN cancers from five anatomical sites, including the pancreas, lung, parathyroid gland, skin and thyroid gland.

Small RNA sequencing of study samples

We generated comprehensive miRNA expression profiles for all samples through barcoded small RNA sequencing.

Table 1. Anatomical distribution and histopathological diagnoses of study samples

NENs	Number of samples, <i>n</i> (%)	non-NENs	Number of samples, <i>n</i> (%)
Total	221		114
Epithelial			
Gastrointestinal tract and pancreas			
PanNET	28 (13%)	PAAD	10 (9%)
INET	31 (14%)		
AppNET	15 (7%)		
RNET	7 (3%)		
Lung			
TC	13 (6%)	LAC	9 (8%) ^a
AC	15 (7%)	LUNG	15 (12%) ^a
SCLC	11 (5%)		
LCNEC	13 (6%)		
Parathyroid gland			
PTA	9 (4%)	PTG	15 (13%)
Pituitary gland			
PitNET	10 (5%)		
Skin			
MCC	17 (8%)	SK	10 (9%)
Thyroid			
MTC	9 (4%)	TG	10 (9%) ^b
		TN	45 (39%) ^b
Non-epithelial			
Adrenal gland and extra-adrenal sites			
NB	25 (11%)		
PCC	10 (5%)		
PGL	8 (4%)		

^aFor lung NENs, neoplastic (LAC) and non-diseased (LUNG) tissue controls were available.

^bFor MTC, neoplastic (TN) and non-diseased (TG) tissue controls were available.

Anatomical location and diagnostic histopathological information are presented for 221 NEN cases, comprising 15 pathological types from seven anatomical sites, and 114 site-matched non-NEN controls, comprising seven diagnostic entities from five anatomical sites. Sample abbreviations: AC, atypical carcinoid; AppNET, appendiceal NET; INET, ileal NET; LCNEC, large-cell NEC; MCC, Merkel cell carcinoma; MTC, medullary thyroid carcinoma; NB, neuroblastoma; PanNET, pancreatic NET; PCC, pheochromocytoma; PGL, paraganglioma; PitNET, pituitary adenoma; PTA, parathyroid adenoma; RNET, rectal NET; SCLC, small-cell lung carcinoma; TC, typical carcinoid. Non-NEN samples comprise lung (LUNG), lung adenocarcinoma (LAC), pancreatic adenocarcinoma (PAAD), parathyroid gland (PTG), skin (SK), thyroid gland (TG) and thyroid neoplasm (TN).

Following sequence annotation, we obtained a median of 4 386 727 (range: 53 516–40 305 4453) total small RNA reads and 258 932 (range: 1312–3 723 507) calibrator reads (Supplementary Table S2). For miRNAs, we detected a median of 2 322 722 (range: 1740–34 781 174) miRNA sequence reads, representing a median of 63.1% total sequence reads; miRNA, miRNA cluster and calibrator expression profiles for each sample were subsequently generated from these reads. Median miRNA content was 26.4 (range: 0.0–2048.4) fmol/ μ g total RNA (Supplementary Table S2).

Abundant miRNA composition in NEN and non-NEN samples

To better understand miRNA composition in NEN and non-NEN samples, we assessed and correlated abundant

miRNAs and miRNA clusters within and between sample sets. Abundant miRNA and miRNA cluster composition was similar within all NEN cases or all non-NEN controls. The number of members in each miRNA cluster is indicated in parentheses following the cluster name, e.g. cluster-hsa-mir-98(13). Among all NEN cases, miR-375, -21, -143, -let-7a, -26a, -7, -let-7f and -125b and cluster-mir-375(1), -98(13), -21(1) and -23a(6) were the most abundant miRNAs and miRNA clusters, with the median relative frequency ranging 1.5–10.6% and 3.6–10.6% of respective total read counts (Supplementary Table S6). Within this group, miR-375, -21, -143, -let-7a, -26a, -7, -let-7f, -125b and -141 and cluster-mir-98(13), -mir-375(1), -mir-7-1(3) and -mir-143(2) were highly expressed in five or more pathological types (Supplementary Table S6). In comparison, among all non-NEN controls, miR-21, -125b, -let-7a, -143, -let-7f, -30a, -26a and -29a and cluster-mir-98(13), -21(1), -30a(4) and -23a(6) were the most abundant miRNA and miRNA clusters, ranging 2.5–10% and 5.2–15.9% of respective total miRNA-annotated read counts (Supplementary Table S7). Within this group, miR-21, -let-7a, -143, -30a, -let-7b and -30d and cluster-mir-98(13), -mir-21(1), -mir-23a(6) and -mir-30a(4) were highly expressed in five or more non-NEN entities (Supplementary Table S7). Correlation analyses highlighted the similarities in abundant miRNA composition within epithelial and non-epithelial NENs; with the exception of PTA, NEN cases were less correlated with site-matched non-NEN controls (Supplementary Figure S1).

Comparative analyses of abundant miRNAs in NEN and non-NEN samples

To better understand meaningful differences in miRNA composition between NEN and non-NEN samples, we compared abundant miRNAs and miRNA clusters for all NEN samples and for each pathological type with relevant controls. Comparative analyses indicated that miR-375 and miR-7 were 216- and 48-fold higher in all NEN cases compared to all non-NEN controls, respectively. Fold changes ranged 59–816- and 41–69-fold higher for miR-375 and miR-7 in specific NEN pathological types compared to site-matched non-NEN controls (Supplementary Table S6 and Figure 1). The only exception was observed in PTA, which showed the lowest miR-375 and miR-7 expression of all NENs; in fact, higher expression was observed in non-neoplastic parathyroid glands. Other notable miRNA overexpression among NENs included miR-127, with 86-fold higher expression in typical carcinoids (TC) compared to lung non-NEN tissues (Supplementary Table S6); cluster-mir-127(8) was also 78-fold higher in TC compared to lung non-NEN tissues (data not shown). In addition, miR-203 and miR-205 expression was 143- and 366-fold higher in non-NEN skin controls than MCC, respectively (Supplementary Table S7).

Unsupervised hierarchical clustering of filtered miRNA expression profiles

To assess the classificatory potential of miRNA expression profiling, we first explored our data using unsupervised hierarchical clustering. With the exception of all PTA

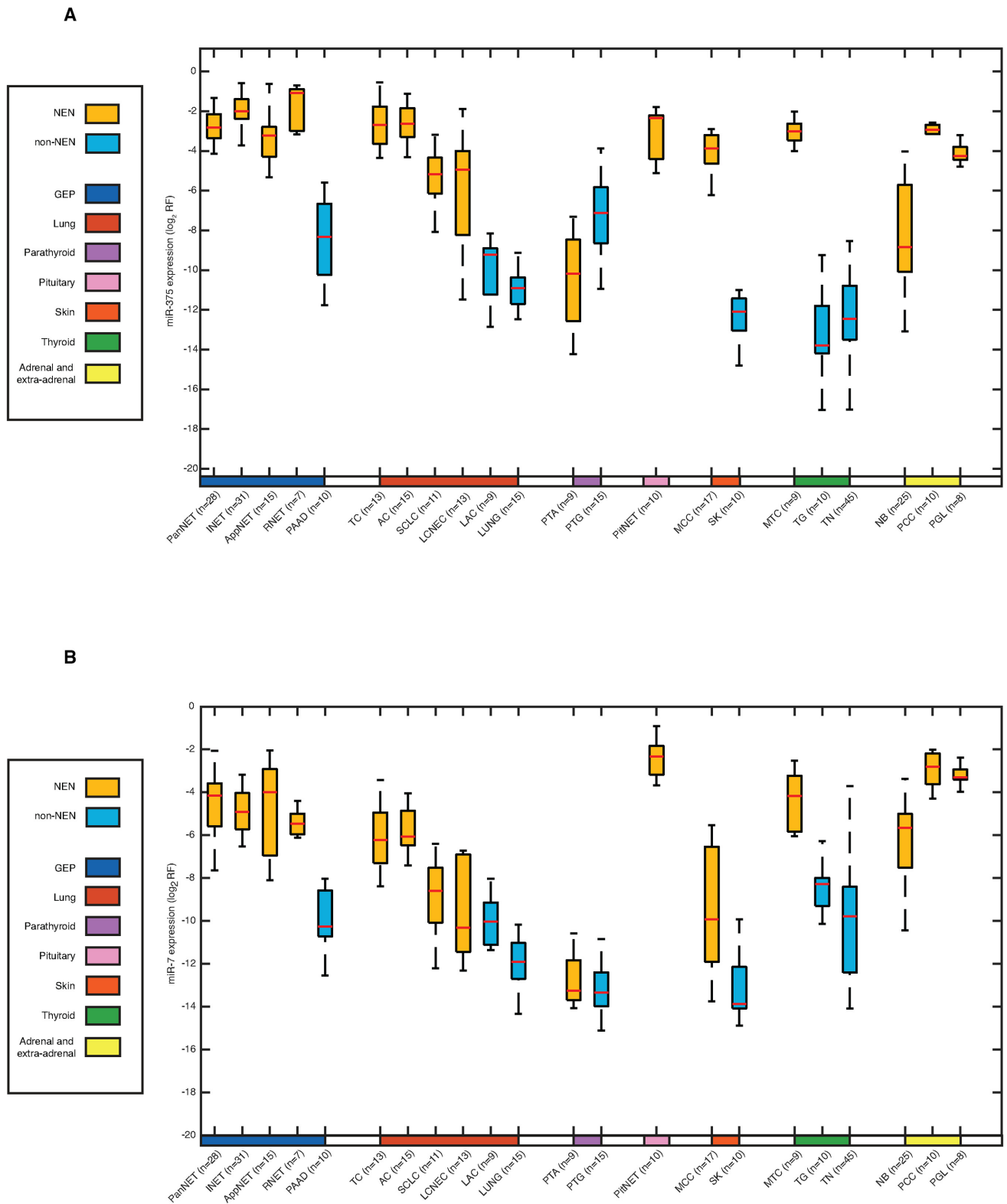


Figure 1. miR-375 and miR-7 expression in NEN and non-NEN samples. Normalized miR-375 and miR-7 expression was examined between 15 NEN pathological types and 7 site-matched non-NEN control groups. Site-matched NEN and non-NEN groups were designated by anatomical site in the color bar: pancreas (blue), lung (red), parathyroid (purple), skin (orange) and thyroid (green); NENs without a site-matched control were left blank. Both miR-375 and miR-7 were higher expressed in NEN cases than non-NEN controls. With the exception of PTA, miR-375 expression was higher in NEN pathological types than in site-matched non-NEN controls. With the exception of PTA, miR-7 was also higher in NEN pathological types compared to site-matched non-NEN controls. Abbreviation: log₂ RF, log₂ normalized relative frequency. Sample abbreviations are provided in Table 1 and Supplementary Table S1.

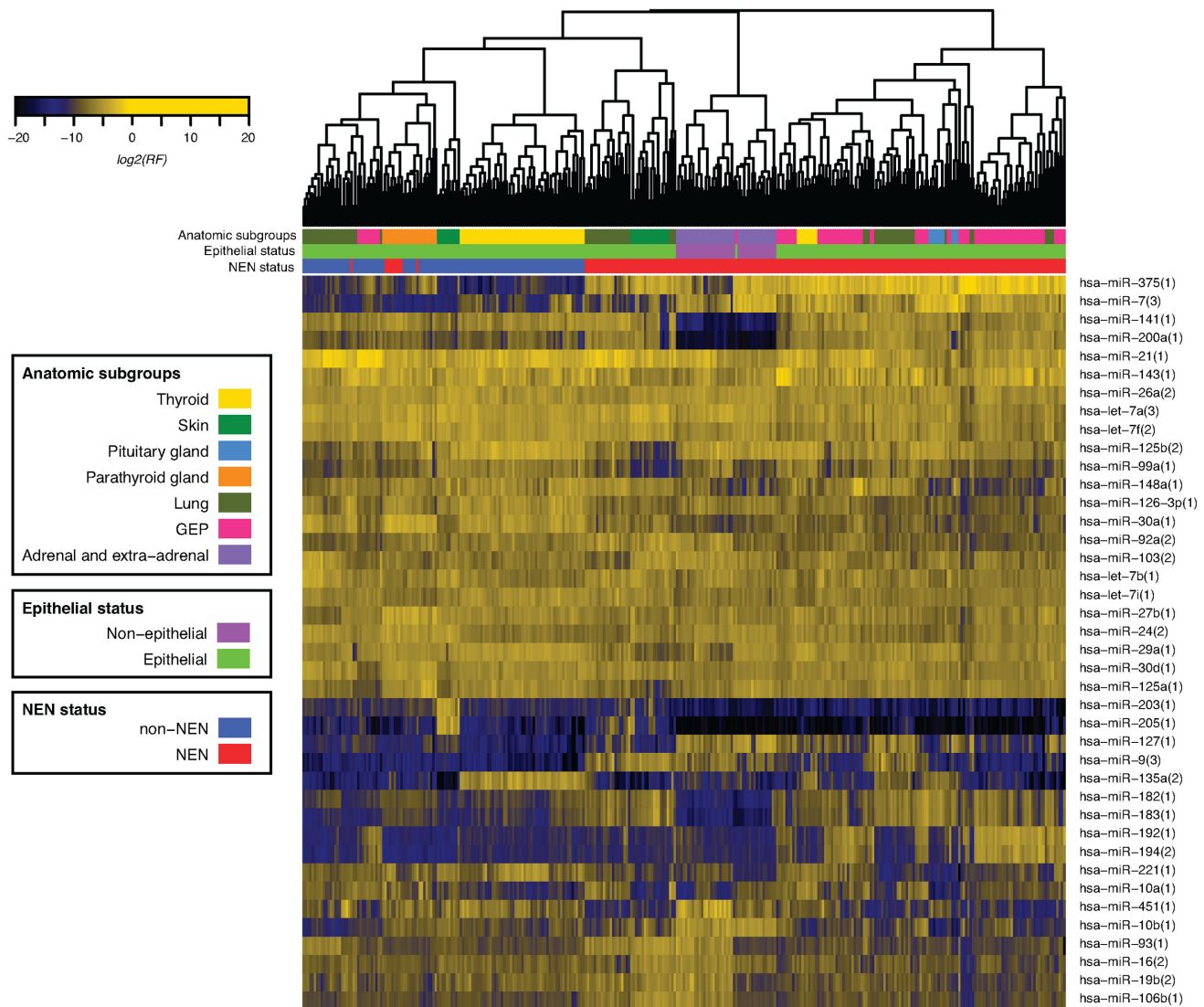


Figure 2. Unsupervised hierarchical clustering of study samples based on miRNA expression. Unsupervised hierarchical clustering using Euclidean distance and complete agglomeration clustering was performed using filtered (union of top 75% abundance) \log_2 normalized miRNA sequence reads for all NEN cases ($n = 221$) and non-NEN controls ($n = 114$). Anatomical groupings comprise the following pathological types described in Table 1 and Supplementary Table S1: thyroid (MTC, TG, TN), skin (MCC, SK), pituitary gland (PitNET), parathyroid gland (PTA, PTG), lung (AC, TC, SCLC, LCNEC, LAC, LUNG), GEP (AppNET, INET, PNET, RNET), and adrenal and extra-adrenal (PCC, PGL). With noted exceptions, NEN cases and non-NEN controls, and epithelial and non-epithelial samples, clustered distinctly and NEN pathological types preferentially clustered with each other than with site-matched non-NEN controls.

samples and one large-cell NEC (LCNEC) sample, NEN cases and non-NEN controls clustered separately (Figure 2). In addition, epithelial samples clustered distinctly from non-epithelial samples with the exception of one pancreatic NET (PanNET). NEN pathological types preferentially clustered together rather than with site-matched non-NEN controls. Unsupervised hierarchical clustering of filtered miRNA cluster expression from the same samples clustered as above (Supplementary Figure S2).

Discovery analyses for miRNA-based NEN classification

Next, we identified candidate miRNA markers for NEN classification using an established approach comprising feature selection and validation (18). Using this approach, we selected effective miRNA markers from the top-ranked

3% miRNAs or miRNA clusters discriminating between or within epithelial or non-epithelial NENs (Supplementary Tables S8 and S9). These comparisons were used to construct and assess the reliability of the multilayer classifier below.

Construction and cross-validation of multilayer classifier

We subsequently constructed and assessed the accuracy of a multilayer miRNA-based classifier for predicting NEN pathological types with 5-fold cross-validation (Figure 3). The resulting classifier consisted of eight decision layers, using the linear or cubic SVM model at each layer (Supplementary Table S10). In the first layer, miR-200a expression was significantly higher in epithelial than non-epithelial NENs (K-W P -value < 0.01); miR-10b provided

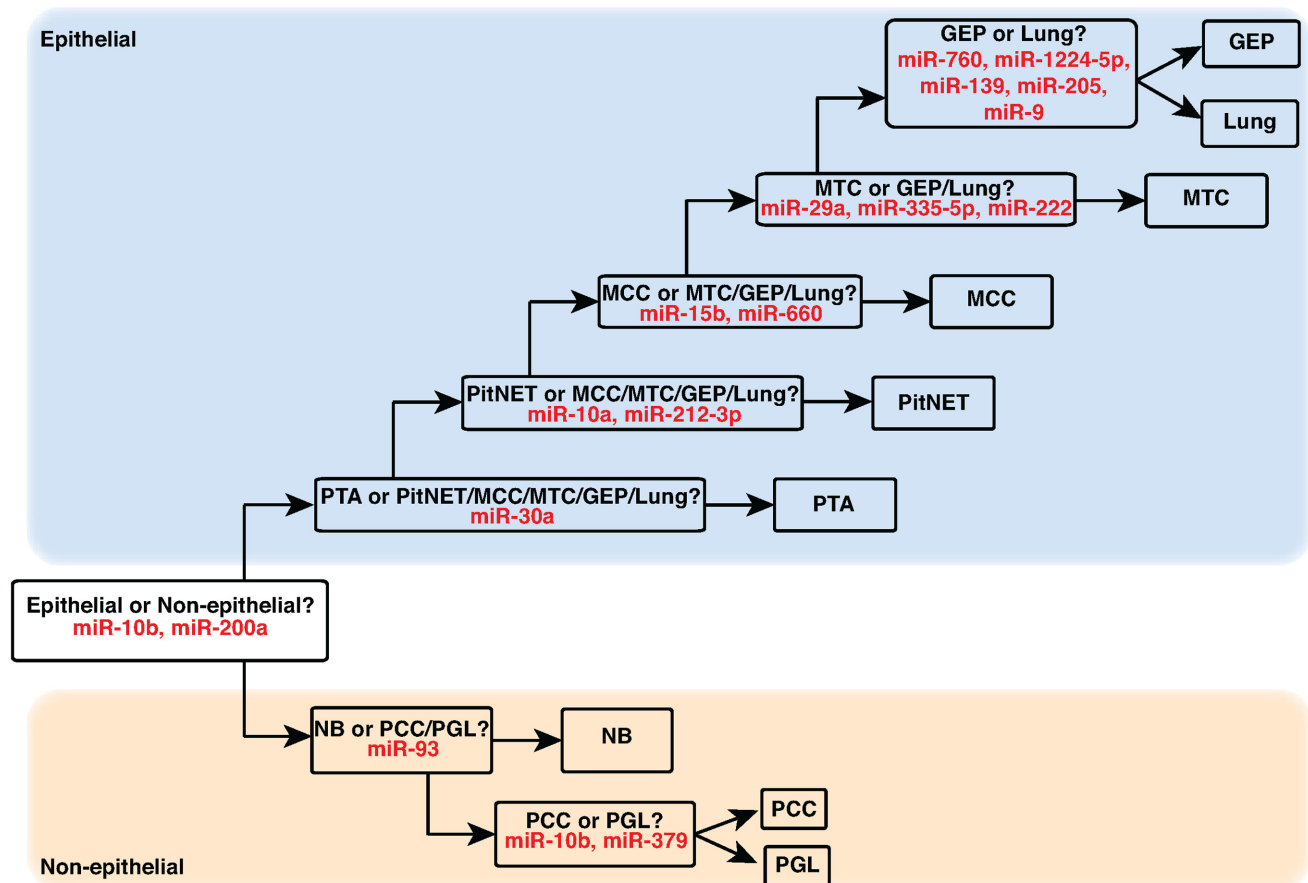


Figure 3. Multilayer miRNA-based classifier for predicting NEN pathological types. A multilayer classifier for predicting NEN pathological types was developed using supervised machine learning models. In the first layer, NEN miRNA profiles were classified as epithelial or non-epithelial based on miR-10b and miR-200a expression. In subsequent layers, epithelial and non-epithelial NENs were successively identified using the selected miRNAs as indicated. Sample abbreviations are provided in Table 1 and Supplementary Table S1.

additional prediction power (K–W P -value <0.01). When combined, these two miRNAs discriminated epithelial and non-epithelial NENs with only one sample misclassification (Figure 4A), which was found to be a histological misidentification (see below). In subsequent layers, sample profiles were successively assigned to other pathological types using the least number of miRNAs required. Within epithelial NENs, PTA, PitNET, MCC and MTC were, respectively, discriminated from remaining NENs based on expression of miR-30a, miR-10a and miR-212-3p, miR-15b and miR-660, and miR-335-5p, miR-29a and miR-222 (Figure 4B–E). Lung NENs and GEP NENs were discriminated based on expression of miR-760, miR-1224-5p, miR-139, miR-205 and miR-9 with three misclassifications (Figure 4F and G). Within non-epithelial NENs, NB and PCC/PGL, and PCC or PGL, were accurately discriminated based on expression of miR-93, and miR-10b and miR-379, respectively (Figure 4H and I). Decision node level accuracy ranged from 97% to 100% (Supplementary Table S10).

Assessment of classifier performance and transferability

Using the 17 miRNAs selected for multilayer classification, t-SNE analysis indicated clear separation of epithelial and non-epithelial NENs with one notable exception (Figure

5), which was found to be a histological misidentification (see below). NEN pathological types also grouped together within epithelial and non-epithelial clusters. With 217 of 221 samples accurately classified, the overall accuracy of our multilayer classifier was 98% (Table 2). miRNA cluster substitutions had little to no effect on overall and decision node level accuracy (data not presented). At each decision node of the classifier, selected miRNAs were always more highly expressed in one comparison group (0.40%; range: 0.01–7.82%) versus the other (0.03%; range: 0.00–2.35%; Supplementary Table S11), highlighting their potential as translatable tissue markers of specific NEN pathological types.

Detection of histological misidentification by miRNA-based NEN classifier

The unusual finding of an epithelial PanNET within the cluster of non-epithelial NENs (Figures 4A and 5), in addition to miRNA-based classification of this PanNET as a PGL (Table 2), prompted us to review the histopathology of this case. Upon review, the tumor was a small (<1 cm in size) low-grade NET at the tail of the pancreas, with histological features overlapping both PanNET and PGL. Immunohistochemical analysis showed that the tumor cells

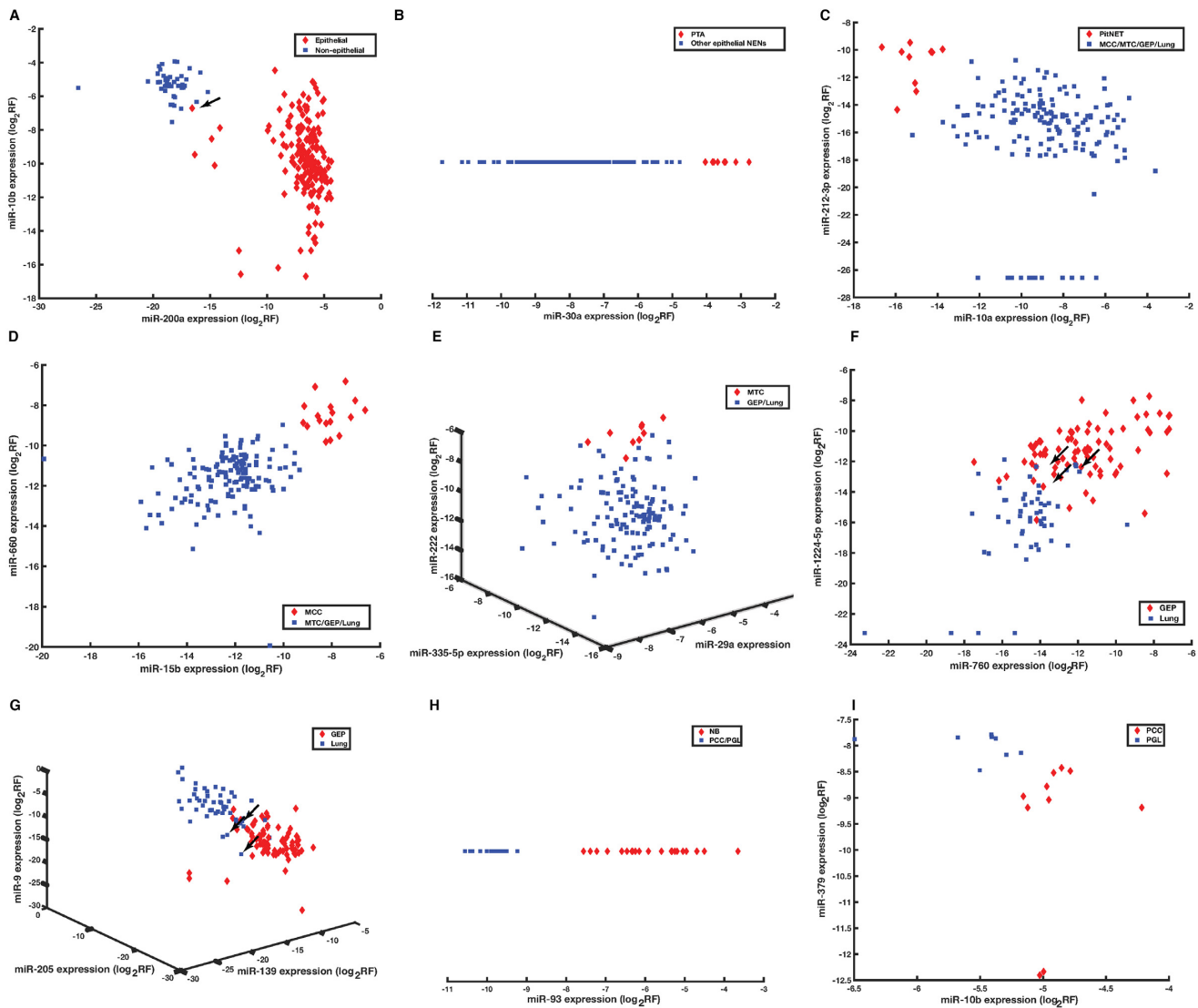


Figure 4. Scatter plot assessment of miRNAs selected for classification. Epithelial and non-epithelial NENs are effectively discriminated based on miR-10b and miR-200a expression with one misclassification (A). Within epithelial NENs, PTA, PitNET, MCC and MTC were accurately discriminated from the remaining NENs based on miR-30a expression (B), miR-10a and miR-212-3p expression (C), miR-15b and miR-660 expression (D), and miR-335-5p, miR-29a and miR-222 expression (E); lung NENs and GEP NENs were discriminated from PCC/PGL based on miR-93 expression (H), and PCC and PGL were separated based on miR-10b and miR-379 expression (I). Similar results were generated using relevant miRNA cluster data and are not presented. Arrows indicate misclassified samples. Abbreviation: \log_2 RF, \log_2 normalized relative frequency. Sample abbreviations are provided in Table 1 and Supplementary Table S1.

were diffusely positive for synaptophysin, chromogranin A and GATA3, and negative for cytokeratin (AE1/AE3 antibodies). This phenotype diagnosed this tumor as a PGL, as predicted by the miRNA classifier, and not a PanNET, which should be cytokeratin-positive and GATA3-negative (23,24). The unusual case was misidentified based on initial histology, but was correctly diagnosed by molecular profiling and miRNA-based classification.

DISCUSSION

Accurate NEN classification is essential for understanding tumor biology and guiding clinical care. NEN pathological classification is modified by experts on an ongoing ba-

sis as updated clinical, pathological, biological and molecular data become available. Recently, these experts proposed a common classification framework for evaluating NENs, clarifying terminology to reduce confusion and harmonizing concepts to facilitate comparisons between pathological types (3). Although morphology-based, this framework is designed to incorporate ‘equally solid genetic studies across all anatomical sites (3)’ over time. Here, we generate biological and clinical insights into NENs through miRNA-based classification.

The strength of our study stems from comparing multiple NEN pathological types and site-matched non-NEN controls using comprehensive miRNA detection through bar-coded small RNA cDNA library sequencing (25) and ac-

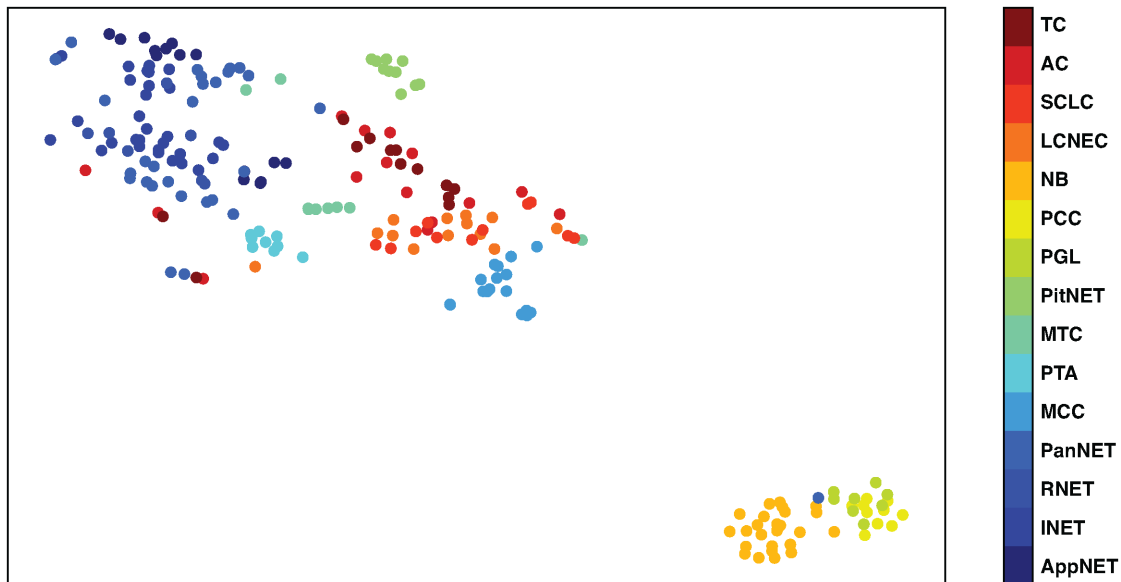


Figure 5. t-SNE for selected classificatory miRNAs. Sample grouping was visually assessed using miRNAs selected for multilayer classification and t-SNE analysis. With one notable exception, samples clustered as epithelial or non-epithelial NENs and tended to group by pathological type. The exception was a misdiagnosed PanNET later found to be a PGL on further testing. Sample abbreviations are provided in Table 1 and Supplementary Table S1.

curate sequence annotation (19). Advanced computational approaches for miRNA feature selection (20) and classifier construction (18) further bolstered our approach. We carefully assessed data reliability through knowledge of miRNA cluster composition (10), evaluated classifier performance and transferability by determining overall and decision node level accuracy, gauged the impact of miRNA cluster substitutions on accuracy and inspected the abundance of selected classificatory miRNAs. Throughout the study, miRNA clusters measured data quality and transferability of miRNAs as clinical markers; we then focused on miRNAs to build a streamlined prototype of a tool for NEN classification. The identified miRNAs can be used as mono-analyte or multi-analyte markers as needed (12).

Unsupervised hierarchical clustering of filtered miRNA expression profiles confirms existing knowledge and provides new knowledge of NEN grouping. With the exception of all PTA and one LCNEC sample, NEN cases and non-NEN controls clustered separately. Based on these findings, we speculate that all PTA have a distinct gene expression pattern linked to their indolent behavior; the LCNEC sample showed areas of possible squamous cell differentiation (data not shown) that may explain peculiar clustering patterns. Within NENs, two major groups corresponding to epithelial and non-epithelial NENs are evident; interestingly, one epithelial NEN clusters with non-epithelial NEN samples. Here, we show that these epithelial and non-epithelial NENs can be discriminated through miR-200a (26) and miR-10b expression, and confirm that our epithelial PanNET sample is actually a non-epithelial PGL based on additional cytokeratin and GATA-3 immunostaining (23,24). Within non-NENs, samples group mostly by anatomical site of origin as expected (6). Visual inspection of cluster diagrams indicates similarities and differ-

ences in abundant miRNA composition in NEN and non-NEN samples.

Similarities in abundant miRNA composition between samples provide coarse insights into cellular gene expression programs. Within NENs, miR-375, -21, -143, -let-7a, -26a, -7, -let-7f, -125b and -141 were highly expressed in five or more pathological types; known oncogenic or tumor suppressor functions for these miRNAs are reviewed elsewhere (8,27). miR-375, the most abundant miRNA in NENs, is believed to regulate lineage-specific differentiation (28–31), growth (32,33) and function (32,34) of neuroendocrine cells. Correlation analyses highlighted similarities in abundant miRNA composition for all NENs, including epithelial or non-epithelial NENs. These findings indicate that all NENs have a constitutive miRNA gene expression program that likely directly or indirectly maintains the neuroendocrine cell phenotype. Given the different cellular origins of epithelial and non-epithelial NENs (35), convergent miRNA gene expression likely implies functional similarities. Within non-NEN samples, miR-21, -let-7a, -143, -30a, -let-7b and -30d were highly expressed in five or more non-NEN entities; their cancer-related functions are reviewed elsewhere as above. While mechanistic insights into cellular processes can be gained through predictable targeting of mRNAs by abundant miRNAs, this topic is beyond the scope of the present study (36).

Differences in abundant miRNA composition between samples can also be used to identify new and confirm known miRNA markers. miR-375 expression was substantially higher in all NEN cases compared to non-NEN controls. Where comparisons allowed, miR-375 was consistently higher in NEN pathological types compared to site-matched non-NEN controls. Based on current miRNA expression tissue atlases, miR-375 is currently thought to be

Table 2. Overall accuracy of multilayer classifier for discriminating NENs

		Established diagnosis								
		GEP NET	Lung NET	MTC	MCC	PitNET	PTA	PCC	PGL	NB
Multilayer classifier designation	GEP NET	80	3							
	Lung NET		49							
	MTC			9						
	MCC				17					
	PitNET					10				
	PTA						9			
	PCC							10		
	PGL	1							8	
	NB									25
Decision-level accuracy		80/81 (99%)	49/52 (94%)	9/9 (100%)	17/17 (100%)	10/10 (100%)	9/9 (100%)	10/10 (100%)	8/8 (100%)	25/25 (100%)
Overall accuracy					217/221 (98%)					

Using our multilayer classifier, NEN miRNA profiles were assigned to one of nine pathological subgroups or pathological types. Cases of GEP NENs (AppNET, INET, PNET, RNET) or lung NENs (TC, AC, SCLC, LCNEC) were not assigned to individual pathological types because we previously developed miRNA-based classifiers for these subgroups (18) (Wong *et al.*, in preparation). By comparing classifier designations to established histopathological diagnoses, we determined our overall classifier accuracy to be 98%. Additional measures of classifier performance were also calculated: precision (0.98), recall (0.99) and Matthews correlation coefficient (0.98). Sample abbreviations are provided in Table 1 and Supplementary Table S1.

an endocrine gland specific marker (6,37). However, the presence of miR-375 in enteroendocrine cells (30,38), pancreatic beta cells (32,33), thyroid C cells (39), and MCC (7,31,40), NB (15) and SCLC cell lines (29) suggests that miR-375 is a neuroendocrine cell marker. Given the specificity and distribution of miR-375 in our samples and its reported abundance in seemingly disparate NEN pathological types (7,18,38,41–43), we propose that miR-375 is a universal marker of neuroendocrine cell differentiation. miR-375 appears to be highly expressed in NENs, in amounts proportional to the number of normal neuroendocrine cells and/or the degree of neuroendocrine differentiation within control tissues or tumors; neuroendocrine differentiation of tumors is more common than currently appreciated (44). More systematic studies are required to confirm this proposal.

Although less abundant than miR-375, miR-7 expression was also elevated in all NEN cases compared to non-NEN controls. Where comparisons allowed, miR-7 was often higher in NEN pathological types compared to site-matched non-NEN controls. Other than expression in the pituitary gland, atlas studies provide limited information on miR-7 expression (6,37). However, the presence of miR-7 in enteroendocrine cells (30), pancreatic islet cells (33,45), thyroid C cells (46), but not controls suggests that this miRNA also has some degree of neuroendocrine specificity. Given their specificity, some tissue profiling studies may have inadvertently interpreted miR-375 or miR-7 reduction in expansile cancer lesions as miRNA reduction rather than neuroendocrine cell destruction. Although miR-127 was higher in TC than non-NEN controls, the significance of this difference is unclear. Conversely, comparisons of abundant miRNA composition between non-NEN and NEN samples identified known tissue-specific miRNA markers such as miR-203 and miR-205 (6).

As with other cancers (4), miRNAs can be used for NEN classification. Using our feature selection algorithm, we identified 17 miRNAs to discriminate 15 NEN pathological types; t-SNE analyses using these miRNAs clearly separated epithelial and non-epithelial NENs and suggested

clustering by pathological type. Given their classificatory potential, we subsequently constructed and validated a multilayer classifier for discriminating NEN pathological types, correctly identifying 217 (98%) of 221 samples. Three of the four misclassified samples occurred at the GEP NEN versus lung NEN decision node, suggesting model overfitting and the need for additional samples for validation. On further testing, the fourth ‘misclassified’ sample turned out to be a PGL as indicated by miRNA expression profiling. We also introduced criteria for evaluating classifier performance and transferability, including determining overall and decision node level accuracy, assessing the impact of miRNA cluster substitutions on classifier accuracy and showing the relative abundance of miRNAs selected for classification.

This study does have limitations that are commonly encountered in rare cancer and miRNA research. Comprehensive clinical information is challenging to obtain, limited sample numbers preclude hold out validation and miRNA content measurements can vary widely due to technical challenges. Nonetheless, we provide compelling evidence that miRNAs are useful for NEN classification and should be included in further multi-omic studies of these neoplasms.

Through comprehensive miRNA expression profiling, we have identified candidate universal and classificatory markers that may be useful as adjunct tissue markers, constructed a multilayer classifier for discriminating NENs and provided reference profiles for hypothesis generation or inter-study comparisons. Our next steps involve confirming our findings in well-annotated sample sets, evaluating miRNAs as circulating markers and investigating upstream promoter activity and downstream targeting events.

DATA AVAILABILITY

Annotated miRNA and miRNA cluster counts (Supplementary Tables S3 and S4) have also been deposited to Data Dryad (<https://datadryad.org/stash/dataset/doi:10.5061/dryad.fn2z34tqj>).

SUPPLEMENTARY DATA

Supplementary Data are available at NAR Cancer Online.

ACKNOWLEDGEMENTS

We wish to thank members of the Rockefeller University Genomics Resource Core and the McGill University and Genome Quebec Innovation Center for outstanding service. We wish to thank Arlene Hurley NP and the Research Facilitation Office staff in The Rockefeller University Center for Clinical and Translational Science for regulatory and administrative assistance.

FUNDING

Academic Health Sciences Center Alternative Funding Plan Innovation Fund; the Canada Foundation for Innovation John R. Evans Leaders Fund; the Carcinoid and Neuroendocrine Tumor Society Canada; the Ontario Research Fund—Research Infrastructure; Robertson Therapeutic Development; The Rockefeller University Center for Clinical and Translational Science Award, funded in part by the National Center for Advancing Translational Sciences, National Institutes of Health Clinical and Translational Science Award program [UL1TR001866]; the South-eastern Ontario Academic Medical Organization; the Ontario Institute of Cancer Research, funded by the Government of Ontario. Funding for open access charge: Ontario Institute of Cancer Research.

Conflict of Interest statement. T. Tuschl is a co-founder of Alnylam Pharmaceuticals and is on the Scientific Advisory Board of Regulus Therapeutics.

REFERENCES

- Wick, M.R. (2000) Neuroendocrine neoplasia. Current concepts. *Am. J. Clin. Pathol.*, **113**, 331–335.
- Kloppel, G. (2017) Neuroendocrine neoplasms: dichotomy, origin and classifications. *Visc. Med.*, **33**, 324–330.
- Rindi, G., Klimstra, D.S., Abedi-Ardekani, B., Asa, S.L., Bosman, F.T., Brambilla, E., Busan, K.J., de Krijger, R.R., Dietel, M., El-Naggar, A.K. *et al.* (2018) A common classification framework for neuroendocrine neoplasms: an International Agency for Research on Cancer (IARC) and World Health Organization (WHO) expert consensus proposal. *Mod. Pathol.*, **31**, 1770–1786.
- Lu, J., Getz, G., Miska, E.A., Alvarez-Saavedra, E., Lamb, J., Peck, D., Sweet-Cordero, A., Ebert, B.L., Mak, R.H., Ferrando, A.A. *et al.* (2005) MicroRNA expression profiles classify human cancers. *Nature*, **435**, 834–838.
- Rosenfeld, N., Aharonov, R., Meiri, E., Rosenwald, S., Spector, Y., Zepeniuk, M., Benjamin, H., Shabes, N., Tabak, S., Levy, A. *et al.* (2008) MicroRNAs accurately identify cancer tissue origin. *Nat. Biotechnol.*, **26**, 462–469.
- Landgraf, P., Rusu, M., Sheridan, R., Sewer, A., Iovino, N., Aravin, A., Pfeffer, S., Rice, A., Kamphorst, A.O., Landthaler, M. *et al.* (2007) A mammalian microRNA expression atlas based on small RNA library sequencing. *Cell*, **129**, 1401–1414.
- Renwick, N., Cekan, P., Masry, P.A., McGeary, S.E., Miller, J.B., Hafner, M., Li, Z., Mihailovic, A., Morozov, P., Brown, M. *et al.* (2013) Multicolor microRNA FISH effectively differentiates tumor types. *J. Clin. Invest.*, **123**, 2694–2702.
- Farazi, T.A., Hoell, J.I., Morozov, P. and Tuschl, T. (2013) MicroRNAs in human cancer. *Adv. Exp. Med. Biol.*, **774**, 1–20.
- Bartel, D.P. (2009) MicroRNAs: target recognition and regulatory functions. *Cell*, **136**, 215–233.
- Farazi, T.A., Brown, M., Morozov, P., Ten Hoeve, J.J., Ben-Dov, I.Z., Hovestadt, V., Hafner, M., Renwick, N., Mihailovic, A., Wessels, L.F. *et al.* (2012) Bioinformatic analysis of barcoded cDNA libraries for small RNA profiling by next-generation sequencing. *Methods*, **58**, 171–187.
- Butz, H. and Patocs, A. (2019) MicroRNAs in endocrine tumors. *EJIFCC*, **30**, 146–164.
- Modlin, I.M., Bodei, L. and Kidd, M. (2016) Neuroendocrine tumor biomarkers: from monoanalytes to transcripts and algorithms. *Best Pract. Res. Clin. Endocrinol. Metab.*, **30**, 59–77.
- Chan, D.L., Clarke, S.J., Diakos, C.I., Roach, P.J., Bailey, D.L., Singh, S. and Pavlakis, N. (2017) Prognostic and predictive biomarkers in neuroendocrine tumours. *Crit. Rev. Oncol. Hematol.*, **113**, 268–282.
- Gustafson, D., Tyryshkin, K. and Renwick, N. (2016) microRNA-guided diagnostics in clinical samples. *Best Pract. Res. Clin. Endocrinol. Metab.*, **30**, 563–575.
- Cheung, I.Y., Farazi, T.A., Ostrovskaya, I., Xu, H., Tran, H., Mihailovic, A., Tuschl, T. and Cheung, N.K. (2014) Deep microRNA sequencing reveals downregulation of miR-29a in neuroblastoma central nervous system metastasis. *Genes Chromosomes Cancer*, **53**, 803–814.
- Shilo, V., Mor-Yosef, I., Abel, R., Mihailovic, A., Wasserman, G., Naveh-Manly, T. and Ben-Dov, I.Z. (2017) Let-7 and microRNA-148 regulate parathyroid hormone levels in secondary hyperparathyroidism. *J. Am. Soc. Nephrol.*, **28**, 2353–2363.
- Mong, E.F., Akat, K.M., Canfield, J., Lockhart, J., Van Wye, J., Matar, A., Tsibris, J.C.M., Wu, J.K., Tuschl, T. and Totary-Jain, H. (2018) Modulation of LIN28B/let-7 signaling by propranolol contributes to infantile hemangioma involution. *Arterioscler. Thromb. Vasc. Biol.*, **38**, 1321–1332.
- Panarelli, N., Tyryshkin, K., Wong, J.J.M., Majewski, A., Yang, X., Scognamiglio, T., Kim, M.K., Bogardus, K., Tuschl, T., Chen, Y.T. *et al.* (2019) Evaluating gastroenteropancreatic neuroendocrine tumors through microRNA sequencing. *Endocr. Relat. Cancer*, **26**, 47–57.
- Brown, M., Suryawanshi, H., Hafner, M., Farazi, T.A. and Tuschl, T. (2013) Mammalian miRNA curation through next-generation sequencing. *Front. Genet.*, **4**, 145.
- Ren, R., Tyryshkin, K., Graham, C.H., Koti, M. and Siemens, D.R. (2017) Comprehensive immune transcriptomic analysis in bladder cancer reveals subtype specific immune gene expression patterns of prognostic relevance. *Oncotarget*, **8**, 70982–71001.
- Kruskal, W.H. and Wallis, W.A. (1952) Use of ranks in one-criterion variance analysis. *J. Am. Stat. Assoc.*, **47**, 583–621.
- Spearman, C. (1906) ‘Footrule’ for measuring correlation. *Br. J. Psychol.*, **2**, 89–108.
- Duan, K. and Mete, O. (2016) Algorithmic approach to neuroendocrine tumors in targeted biopsies: practical applications of immunohistochemical markers. *Cancer Cytopathol.*, **124**, 871–884.
- Uccella, S., La Rosa, S., Volante, M. and Papotti, M. (2018) Immunohistochemical biomarkers of gastrointestinal, pancreatic, pulmonary, and thymic neuroendocrine neoplasms. *Endocr. Pathol.*, **29**, 150–168.
- Hafner, M., Renwick, N., Farazi, T.A., Mihailovic, A., Pena, J.T. and Tuschl, T. (2012) Barcoded cDNA library preparation for small RNA profiling by next-generation sequencing. *Methods*, **58**, 164–170.
- Park, S.M., Gaur, A.B., Lengyel, E. and Peter, M.E. (2008) The miR-200 family determines the epithelial phenotype of cancer cells by targeting the E-cadherin repressors ZEB1 and ZEB2. *Genes Dev.*, **22**, 894–907.
- Svoronos, A.A., Engelman, D.M. and Slack, F.J. (2016) OncomiR or tumor suppressor? The duplicity of microRNAs in cancer. *Cancer Res.*, **76**, 3666–3670.
- Kloosterman, W.P., Lagendijk, A.K., Ketting, R.F., Moulton, J.D. and Plasterk, R.H. (2007) Targeted inhibition of miRNA maturation with morpholinos reveals a role for miR-375 in pancreatic islet development. *PLoS Biol.*, **5**, e203.
- Nishikawa, E., Osada, H., Okazaki, Y., Arima, C., Tomida, S., Tatematsu, Y., Taguchi, A., Shimada, Y., Yanagisawa, K., Yatabe, Y. *et al.* (2011) miR-375 is activated by ASH1 and inhibits YAP1 in a lineage-dependent manner in lung cancer. *Cancer Res.*, **71**, 6165–6173.
- Knudsen, L.A., Petersen, N., Schwartz, T.W. and Egerod, K.L. (2015) The microRNA repertoire in enteroendocrine cells: identification of

- miR-375 as a potential regulator of the enteroendocrine lineage. *Endocrinology*, **156**, 3971–3983.
31. Abraham, K.J., Zhang, X., Vidal, R., Pare, G.C., Feilotter, H.E. and Tron, V.A. (2016) Roles for miR-375 in neuroendocrine differentiation and tumor suppression via notch pathway suppression in Merkel cell carcinoma. *Am. J. Pathol.*, **186**, 1025–1035.
 32. Poy, M.N., Hausser, J., Trajkovski, M., Braun, M., Collins, S., Rorsman, P., Zavolan, M. and Stoffel, M. (2009) miR-375 maintains normal pancreatic alpha- and beta-cell mass. *Proc. Natl Acad. Sci. U.S.A.*, **106**, 5813–5818.
 33. Latreille, M., Herrmanns, K., Renwick, N., Tuschl, T., Malecki, M.T., McCarthy, M.I., Owen, K.R., Rulicke, T. and Stoffel, M. (2015) miR-375 gene dosage in pancreatic beta-cells: implications for regulation of beta-cell mass and biomarker development. *J. Mol. Med. (Berl.)*, **93**, 1159–1169.
 34. Zhang, N., Lin, J.K., Chen, J., Liu, X.F., Liu, J.L., Luo, H.S., Li, Y.Q. and Cui, S. (2013) MicroRNA 375 mediates the signaling pathway of corticotropin-releasing factor (CRF) regulating pro-opiomelanocortin (POMC) expression by targeting mitogen-activated protein kinase 8. *J. Biol. Chem.*, **288**, 10361–10373.
 35. Kloppel, G. (2017) Neuroendocrine neoplasms: dichotomy, origin and classifications. *Visc. Med.*, **33**, 324–330.
 36. Bartel, D.P. (2018) Metazoan microRNAs. *Cell*, **173**, 20–51.
 37. Ludwig, N., Leidinger, P., Becker, K., Backes, C., Fehlmann, T., Pallasch, C., Rheinheimer, S., Meder, B., Stahler, C., Meese, E. *et al.* (2016) Distribution of miRNA expression across human tissues. *Nucleic Acids Res.*, **44**, 3865–3877.
 38. Arvidsson, Y., Rehammar, A., Bergstrom, A., Andersson, E., Altiparmak, G., Sward, C., Wangberg, B., Kristiansson, E. and Nilsson, O. (2018) miRNA profiling of small intestinal neuroendocrine tumors defines novel molecular subtypes and identifies miR-375 as a biomarker of patient survival. *Mod. Pathol.*, **31**, 1302–1317.
 39. Romeo, P., Colombo, C., Granata, R., Calareso, G., Gualeni, A.V., Dugo, M., De Cecco, L., Rizzetti, M.G., Zanframundo, A., Aiello, A. *et al.* (2018) Circulating miR-375 as a novel prognostic marker for metastatic medullary thyroid cancer patients. *Endocr. Relat. Cancer*, **25**, 217–231.
 40. Fan, K., Ritter, C., Nghiem, P., Blom, A., Verhaegen, M.E., Dlugosz, A., Odum, N., Woetmann, A., Tohill, R.W., Hicks, R.J. *et al.* (2018) Circulating cell-free miR-375 as surrogate marker of tumor burden in Merkel cell carcinoma. *Clin. Cancer Res.*, **24**, 5873–5882.
 41. Hudson, J., Duncavage, E., Tamburrino, A., Salerno, P., Xi, L., Raffeld, M., Moley, J. and Chernock, R.D. (2013) Overexpression of miR-10a and miR-375 and downregulation of YAP1 in medullary thyroid carcinoma. *Exp. Mol. Pathol.*, **95**, 62–67.
 42. Galuppini, F., Bertazza, L., Barollo, S., Cavedon, E., Rugge, M., Guzzardo, V., Sacchi, D., Watutantrige-Fernando, S., Vianello, F., Mian, C. *et al.* (2017) MiR-375 and YAP1 expression profiling in medullary thyroid carcinoma and their correlation with clinical-pathological features and outcome. *Virchows Arch.*, **471**, 651–658.
 43. Miller, H.C., Frampton, A.E., Malczewska, A., Ottaviani, S., Stronach, E.A., Flora, R., Kaemmerer, D., Schwach, G., Pfragner, R., Faiz, O. *et al.* (2016) MicroRNAs associated with small bowel neuroendocrine tumours and their metastases. *Endocr. Relat. Cancer*, **23**, 711–726.
 44. La Rosa, S., Sessa, F. and Uccella, S. (2016) Mixed neuroendocrine–nonneuroendocrine neoplasms (MiNENs): unifying the concept of a heterogeneous group of neoplasms. *Endocr. Pathol.*, **27**, 284–311.
 45. Joglekar, M.V., Joglekar, V.M. and Hardikar, A.A. (2009) Expression of islet-specific microRNAs during human pancreatic development. *Gene Expr. Patterns*, **9**, 109–113.
 46. Santarpia, L., Calin, G.A., Adam, L., Ye, L., Fusco, A., Giunti, S., Thaller, C., Paladini, L., Zhang, X., Jimenez, C. *et al.* (2013) A miRNA signature associated with human metastatic medullary thyroid carcinoma. *Endocr. Relat. Cancer*, **20**, 809–823.

Loss of *YAP1* defines neuroendocrine differentiation of lung tumors

Takeshi Ito,¹ Daisuke Matsubara,^{1,2} Ichidai Tanaka,³ Kanae Makiya,¹ Zen-ichi Tanei,¹ Yuki Kumagai,¹ Shu-Jen Shiu,¹ Hiroki J. Nakaoka,¹ Shumpei Ishikawa,⁴ Takayuki Isagawa,⁴ Teppei Morikawa,⁵ Aya Shinozaki-Ushiku,⁵ Yasushi Goto,⁶ Tomoyuki Nakano,⁷ Takehiro Tsuchiya,⁸ Hiroyoshi Tsubochi,⁹ Daisuke Komura,¹⁰ Hiroyuki Aburatani,¹⁰ Yoh Dobashi,¹¹ Jun Nakajima,⁸ Shunsuke Endo,⁷ Masashi Fukayama,⁵ Yoshitaka Sekido,³ Toshiro Niki² and Yoshinori Murakami¹

¹Molecular Pathology Laboratory, Institute of Medical Science, University of Tokyo, Tokyo; ²Department of Integrative Pathology, Jichi Medical University, Tochigi; ³Division of Molecular Oncology, Aichi Cancer Center Research Institute, Aichi; ⁴Department of Genomic Pathology, Medical Research Institute, Tokyo Medical and Dental University, Tokyo; ⁵Departments of ⁵Human Pathology; ⁶Respiratory Medicine, Graduate School of Medicine, University of Tokyo, Tokyo; ⁷Department of Thoracic Surgery, Jichi Medical University, Tochigi; ⁸Department of Thoracic Surgery, University of Tokyo, Tokyo; ⁹Department of Thoracic Surgery, Jichi Medical University Saitama Medical Center, Saitama; ¹⁰Division of Genome Science, Research Center for Advanced Science and Technology, University of Tokyo, Tokyo; ¹¹Department of Pathology, Jichi Medical University Saitama Medical Center, Saitama, Japan

Key words

Chemosensitivity, Hippo pathway, neuroendocrine differentiation, small-cell lung cancer, *YAP1*

Correspondence

Daisuke Matsubara, Division of Molecular Pathology, Department of Cancer Biology, Institute of Medical Science, University of Tokyo, 4-6-1, Shirokanedai, Minato-ku, Tokyo 108-8639, Japan.
Tel.: +81-3-5449-5260; Fax: +81-3-5449-5407;
E-mail: vzv07574@nifty.com

Funding Information

Japan Society for the Promotion of Science (KAKENHI grant nos. 16K08672, 90198424, 25460432, and 30182108); Ministry of Health, Labor, and Welfare of Japan; Smoking Research Foundation; Foundation for the Development of the Community.

Received April 18, 2016; Revised June 21, 2016; Accepted July 12, 2016

Cancer Sci 107 (2016) 1527–1538

doi: 10.1111/cas.13013

YAP1, the main Hippo pathway effector, is a potent oncogene and is overexpressed in non-small-cell lung cancer (NSCLC); however, the *YAP1* expression pattern in small-cell lung cancer (SCLC) has not yet been elucidated in detail. We report that the loss of *YAP1* is a special feature of high-grade neuroendocrine lung tumors. A hierarchical cluster analysis of 15 high-grade neuroendocrine tumor cell lines containing 14 SCLC cell lines that depended on the genes of Hippo pathway molecules and neuroendocrine markers clearly classified these lines into two groups: the *YAP1*-negative and neuroendocrine marker-positive group ($n = 11$), and the *YAP1*-positive and neuroendocrine marker-negative group ($n = 4$). Among the 41 NSCLC cell lines examined, the loss of *YAP1* was only observed in one cell line showing the strong expression of neuroendocrine markers. Immunostaining for *YAP1*, using the sections of 189 NSCLC, 41 SCLC, and 30 large cell neuroendocrine carcinoma (LCNEC) cases, revealed that the loss of *YAP1* was common in SCLC (40/41, 98%) and LCNEC (18/30, 60%), but was rare in NSCLC (6/189, 3%). Among the SCLC and LCNEC cases tested, the loss of *YAP1* correlated with the expression of neuroendocrine markers, and a survival analysis revealed that *YAP1*-negative cases were more chemosensitive than *YAP1*-positive cases. Chemosensitivity test for cisplatin using *YAP1*-positive/*YAP1*-negative SCLC cell lines also showed compatible results. *YAP1*-sh-mediated knockdown induced the neuroendocrine marker *RAB3a*, which suggested the possible involvement of *YAP1* in the regulation of neuroendocrine differentiation. Thus, we showed that the loss of *YAP1* has potential as a clinical marker for predicting neuroendocrine features and chemosensitivity.

In the 2015 WHO classification, SCLC and LCNEC have been categorized together as high-grade neuroendocrine tumors,⁽¹⁾ which are highly aggressive tumors with a poor prognosis. Although high-grade neuroendocrine tumors respond to platinum-based chemotherapy,^(2–7) a cure is sometimes difficult to achieve because these tumors are likely to be widely disseminated by the time of diagnosis. In spite of the many challenges associated with identifying potential targeted therapies, no targeted agents had been approved for use in the treatment of SCLC and LCNEC cases until very recently. Therefore, the mechanisms underlying carcinogenesis in high-grade neuroendocrine tumors need to be elucidated in more detail, and improvements in the therapies for these tumors are desired.

It has become increasingly apparent that abnormalities in the upstream and downstream members of the Hippo pathway play important roles in the tumorigenesis of various human

cancers.⁽⁸⁾ The Hippo pathway has been implicated in the cell contact inhibition of proliferation as well as organ size control.⁽⁹⁾ As the main downstream effector of the Hippo pathway, *YAP1* promotes cell growth as a transcription cofactor and may be inactivated through its cytoplasmic retention and phosphorylation by LATS1/2.^(10,11) The *YAP1* gene was previously reported to be amplified and overexpressed in several tumor types.^(12–16) The overexpression of *YAP1* has also frequently been observed in NSCLC, and is a poor prognostic factor.⁽¹⁴⁾ Few studies have focused on *YAP1* in SCLC; Wu *et al.*'s⁽¹⁷⁾ study identified some single nucleotide polymorphisms within the promoter region of *YAP1* that were associated with the survival of SCLC patients, and Nishikawa *et al.*⁽¹⁸⁾ reported the inhibition of *YAP1* by ASCL1 through the activation of mir375. These findings suggest the importance of *YAP1* in high-grade neuroendocrine tumors; however, its role in neuroendocrine differentiation currently remains unknown, and an

Table 1. Histological types and sources of 24 lung carcinomas

Cell line	Histological type	Cell type	Source
H69	Small-cell lung cancer	Floating	ATCC (Manassas, VA, USA)
H146	Small-cell lung cancer	Floating	ATCC
H510A	Small-cell lung cancer	Floating	ATCC
H889	Small-cell lung cancer	Floating	ATCC
N417	Small-cell lung cancer	Floating	ATCC
H2081	Small-cell lung cancer	Floating	ATCC
H446	Small-cell lung cancer	Floating	ATCC
H526	Small-cell lung cancer	Floating	ATCC
Lu130	Small-cell lung cancer	Floating	Japanese Cancer Research Resources Bank (Osaka, Japan)
Lu135	Small-cell lung cancer	Floating	Japanese Cancer Research Resources Bank
Lu139	Small-cell lung cancer	Floating	Japanese Cancer Research Resources Bank
SBC3	Small-cell lung cancer	Adherent	Japanese Cancer Research Resources Bank
SBC5	Small-cell lung cancer	Adherent	Japanese Cancer Research Resources Bank
RERF-LC-MA	Small-cell lung cancer	Adherent	Japanese Cancer Research Resources Bank
H460	Large-cell carcinoma	Adherent	ATCC
A549	Adenocarcinoma	Adherent	Japanese Cancer Research Resources Bank
ABC-1	Adenocarcinoma	Adherent	Japanese Cancer Research Resources Bank
LC-2/ad	Adenocarcinoma	Adherent	RIKEN Cell Bank (Tsukuba, Japan)
VMRC-LCD	Adenocarcinoma	Adherent	Japanese Cancer Research Resources Bank
H292	Adenocarcinoma	Adherent	ATCC
H441	Adenocarcinoma	Adherent	ATCC
H1651	Adenocarcinoma	Adherent	ATCC
H596	Adenosquamous cell carcinoma	Adherent	ATCC

immunohistochemical analysis of YAP1 using SCLC and LCNEC tissue sections has not yet been undertaken.

In the present study, we report the potential of the loss of YAP1 as a clinical marker to predict neuroendocrine features and chemosensitivity. As far as we know, this study is the first

Table 2. Antibodies used for Western blot analysis of lung cancer cell lines

Antibody	Source
YAP (D8H1X)	Cell Signaling Technology, (Danvers, MA, USA)
AMOTL2 (N-14)	Santa Cruz Biotechnology
AJUBA	Cell Signaling Technology
NCAM (H-300)	Santa Cruz Biotechnology
Chromogranin A (LK2H10)	Abcam, (Cambridge, UK)
Synaptophysin (ab53166)	Abcam
RAB3A (K-15)	Santa Cruz Biotechnology
α -Tubulin (TU-02)	Santa Cruz Biotechnology
GAPDH (V-18)	Santa Cruz Biotechnology

to reveal the roles of YAP1 not only in cisplatin resistance but also in determination of neuroendocrine features of high-grade neuroendocrine tumors.

Materials and Methods

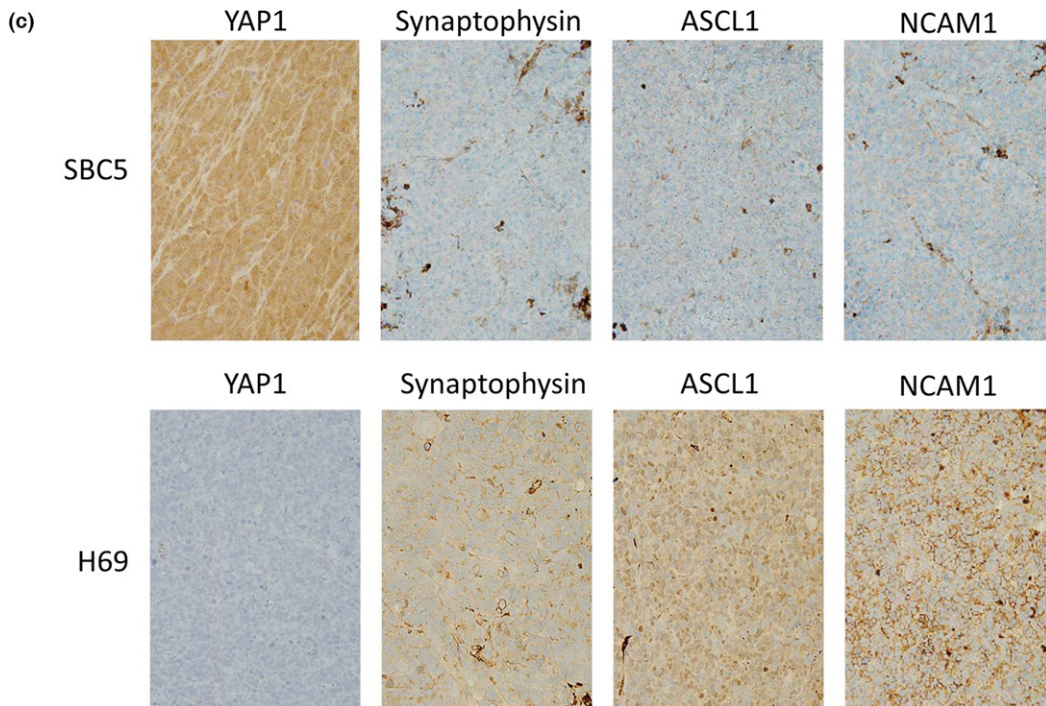
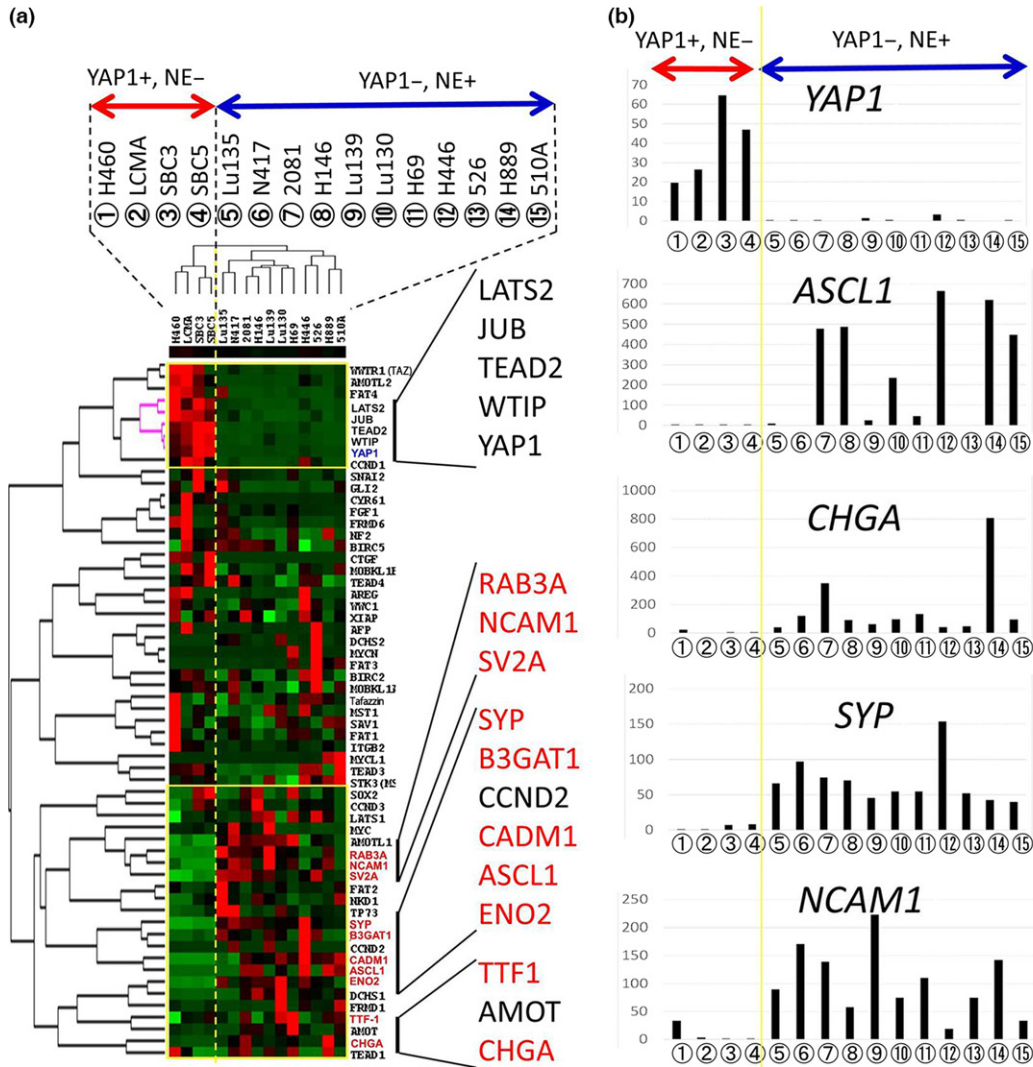
Cell lines and medium. Fourteen SCLC cell lines (SBC3, SBC5, LCMA, Lu135, N417, H2081, H146, Lu139, Lu130, H69, H446, H526, H889, and H510A), seven adenocarcinoma cell lines (A549, ABC1, LC-2/ad, VMRC-LCD, H292, H441, and H1651), one adenosquamous cell carcinoma cell line (H596), and one large-cell carcinoma (H460) were used for Western blot and/or gene expression analyses per mRNA-Seq. H460, derived as a large-cell carcinoma, has been regarded as a LCNEC cell line in some studies.^(19,20) The 14 SCLC cell lines and H460 cell line are described as 15 high-grade neuroendocrine tumor cell lines in the present study for convenience. All cell lines were maintained in RPMI-1640 supplemented with 10% FCS, glutamine, and antibiotics in a humidified atmosphere with 5% CO₂ and 95% air. The sources and histological types of these cell lines are detailed in Table 1.

Gene expression analysis per transcriptome sequencing. Gene expression analysis of the 15 high-grade neuroendocrine tumor cell lines was carried out per mRNA-Seq using an Illumina GAIIx sequencer (Illumina, San Diego, CA, USA). Details are shown in Appendix S1.

Oligonucleotide array analysis data. We used the gene expression data of the oligonucleotide array analysis on 41 NSCLC cell lines including H460 obtained in our previous studies.^(21–23) The sources and histological types of these cell lines are detailed in our previous study.⁽²²⁾

Western blot analysis. Western blot analysis was carried out as previously described.⁽²⁴⁾ Briefly, cell lysates were prepared from lung cancer cell lines using a lysis buffer containing a protease inhibitor mixture (200 μ M 4-(2-aminoethyl) benzene-sulfonyl fluoride, 10 μ M leupeptin, and 1 μ M pepstatin A). Equal amounts of total protein (20 μ g) were fractionated in 7.5% SDS-PAGE, transferred to a PVDF membrane (Millipore, Bedford, MA, USA), and incubated with an appropriate

Fig. 1. (a) Hierarchical cluster analysis of 15 high-grade neuroendocrine lung tumor cell lines using the gene expression of Hippo pathway-correlated molecules and neuroendocrine differentiation-correlated molecules including neuroendocrine markers and the myc family. The genes of neuroendocrine markers are shown in red text. The red bar indicates YAP1-positive and neuroendocrine marker-negative cell lines ($n = 4$); blue bars indicate YAP1-negative and neuroendocrine marker-positive cell lines ($n = 11$). (b) Gene expression levels of neuroendocrine markers (YAP1, ASCL1, CHGA, SYP, and NCAM1) in 15 high-grade neuroendocrine lung tumor cell lines. The numbers enclosed in circles correspond to the cell lines shown in (a). (c) Immunohistochemical expression patterns of YAP1, synaptophysin, NCAM1, and ASCL1 of a representative YAP1-positive SCLC cell line (SBC5) and representative YAP1-negative SCLC cell line (H69) under a high-power view field ($\times 400$).



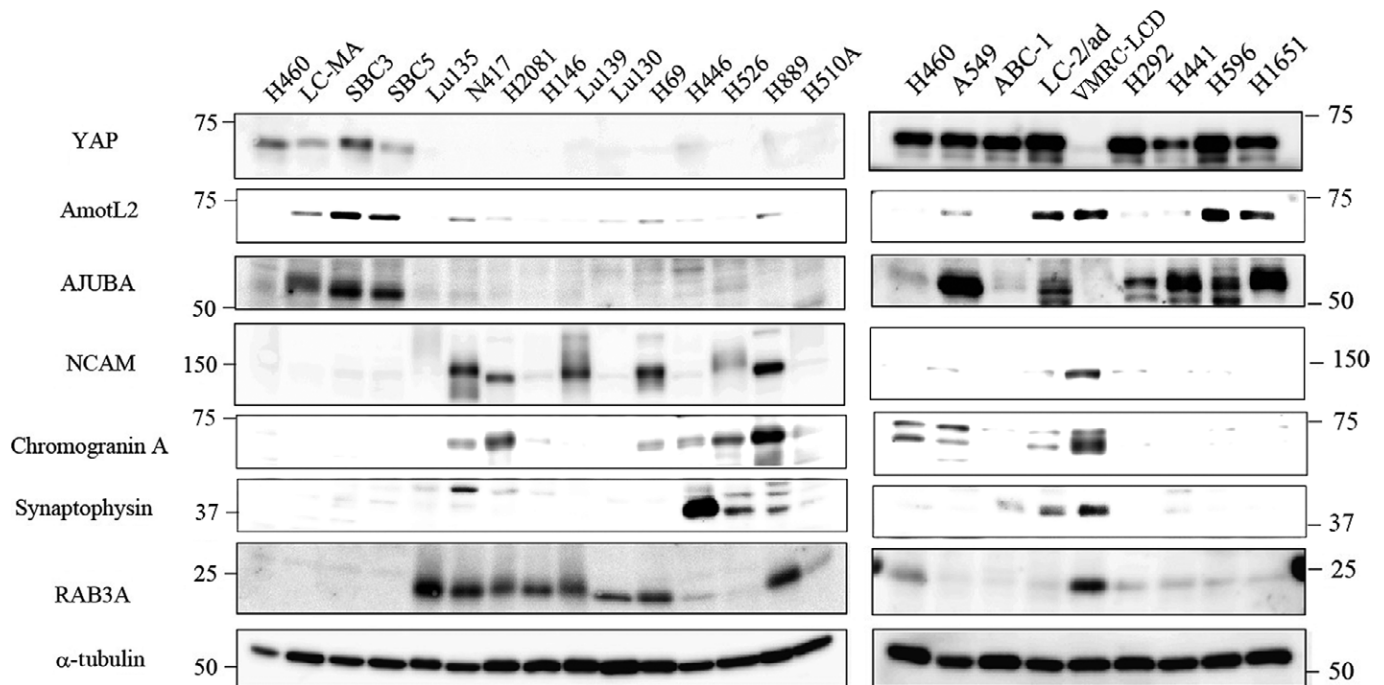


Fig. 2. Western blot analysis of gene products selectively expressed in YAP1-positive and YAP1-negative groups using 15 high-grade neuroendocrine lung tumor cell lines (left panel) and 9 non-small-cell lung cancer cell lines (right panel). YAP1, AMOTL2, and AJUBA are Hippo pathway-correlated molecules and synaptophysin, ASCL1, chromogranin A, and RAB3A are neuroendocrine markers.

Table 3. Immunohistochemical positivity for YAP1, chromogranin A, synaptophysin, NCAM1, and ASCL1 of xenograft tumors of eight lung cancer cell lines

	YAP1	ASCL1	Synaptophysin	Chromogranin A	NCAM1
H460†	+	-	-	-	-
SBC5†	+	-	-	-	-
N417‡	-	-	+	-	+
2081‡	-	+	+	-	+
H69‡	-	+	+	-	+
510A‡	-	+	+	-	+
Lu135‡	-	+	-	-	+
H146‡	-	+	+	-	+

†YAP1-positive cell lines. ‡YAP1-negative cell lines.

antibody. The binding of the primary antibody was detected with the ECL Western Blotting Detection Reagent (GE Healthcare, Chalfont St. Giles, UK) using a peroxidase-conjugated secondary antibody (GE Healthcare). The sources of the antibodies used in this study are summarized in Table 2.

Tissue microarray sections. We used TMAs that were produced to accommodate primary lung cancer tissue core sections collected from patients ($n = 201$) who had undergone surgical resection at the University of Tokyo Hospital (Tokyo, Japan) between 2005 and 2008. Of the 201 core sections examined, 142 were adenocarcinomas, 40 were squamous cell carcinomas, 7 were pleomorphic carcinomas, 6 were SCLCs, and 6 were LCNECs. Informed consent was obtained from all patients, and the study was approved by the Institutional Ethics Review Committee.

Whole sections of high-grade pulmonary neuroendocrine tumors. Tumor specimens were obtained from 71 patients (41 SCLCs and 30 LCNECs) who underwent lung cancer surgery

at the Jichi Medical University Hospital (Tochigi, Japan), the Jichi Medical University Saitama Medical Center (Saitama, Japan), and the University of Tokyo Hospital. Among 71 cases, 7 were treated with platinum-based neo-adjuvant chemotherapy (CDDP + GEM [$n = 2$], CDDP + VP16 [$n = 3$], CDDP + VNR [$n = 1$], and CDDP + docetaxel [$n = 1$]), 63 cases were not treated with neo-adjuvant chemotherapy, and one case was unknown. Among the 63 cases not treated with neo-adjuvant chemotherapy, 33 cases were treated with platinum-based adjuvant chemotherapy (CBDCA + CPT11 [$n = 2$], CBDCA + GEM [$n = 1$], CBDCA + VNR [$n = 1$], CBDCA + VP16 [$n = 17$], CDDP + VNR [$n = 1$], CDDP + CBDCA + vindesine [$n = 1$], CDDP + CBDCA + VP16 [$n = 1$], CDDP + CPT11 [$n = 1$], CDDP + picibanil [$n = 1$], CDDP + CPT11 + VP16 [$n = 1$], and CDDP + VP16 [$n = 6$]), only one case was treated with CAV chemotherapy, 28 cases were not treated with platinum-based or CAV chemotherapy, and one case was unknown. Details are shown in Appendix S1. Informed consent was obtained from all patients, and the study was approved by the Institutional Ethics Review Committee.

Xenograft tumors of SCLC/NSCLC cell lines. We established xenograft tumors of SCLC/NSCLC cell lines by injecting cell suspensions (1×10^7) into the flanks of 6-week-old female nude mice (BALB/c nu/nu).

Immunohistochemistry and evaluation. Formalin-fixed, paraffin-embedded tumor specimens were analyzed by immunohistochemistry using antibodies to YAP1, synaptophysin, chromogranin A, NCAM, and ASCL1. The sources of antibodies, staining procedures, and evaluation methods are given in Appendix S1. In brief, the expression of each neuroendocrine marker antibody in a tumor was defined as positive when 10% of the tumor cells or greater were stained, and negative when less than 10% were stained. The expression of the YAP1

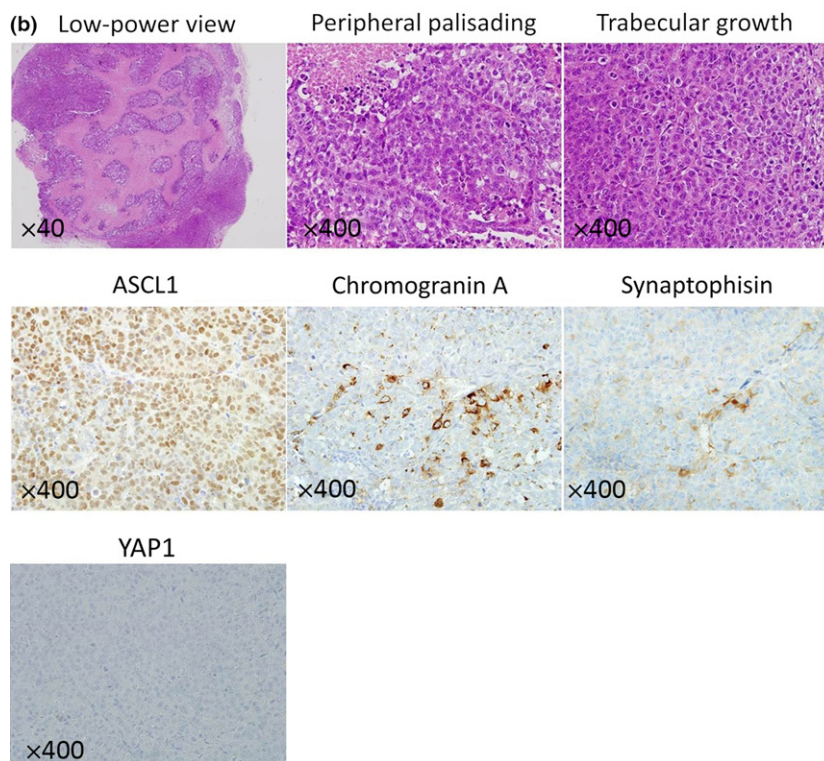
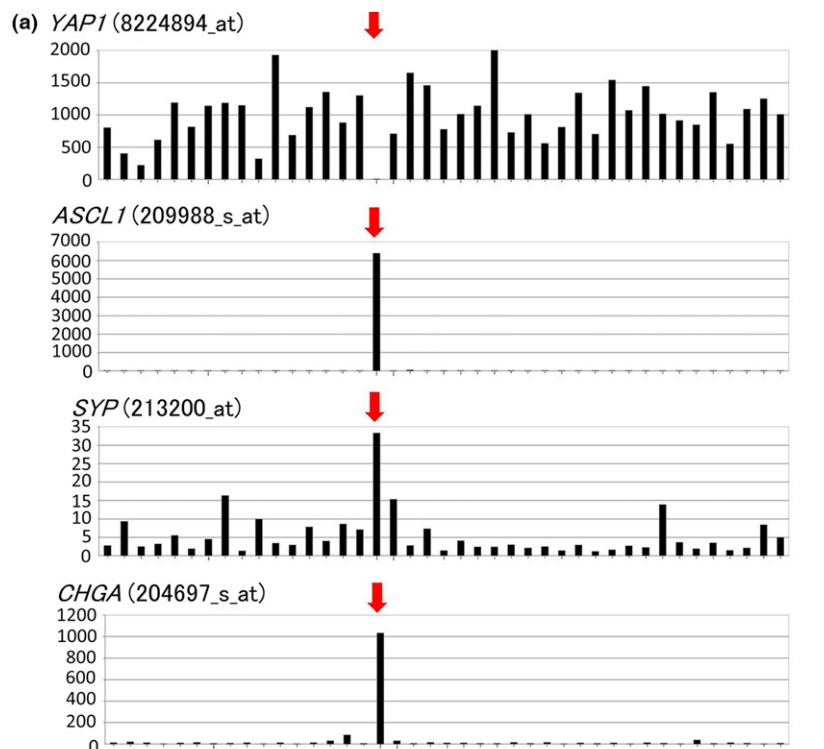


Fig. 3. (a) *YAP1* gene expression levels (8224894_at), *ASCL1* gene expression levels (209988_s_at), *SYP* gene expression levels (213200_at), and *CHGA* gene expression levels (204697_s_at) in 41 NSCLC cell lines including VMRC-LCD (red arrows). (b) Histopathology of xenograft tumors of the VMRC-LCD cell line. Top left panel: HE section in a low-power view field (×40) showing that VMRC-LCD cells proliferate to form solid nests with extensive necrosis. Top center and top right panels: HE sections in a high-power view field (×400). VMRC-LCD cells, having large nuclei with prominent nucleoli and a more abundant cytoplasm than SCLC, showed solid growth patterns with peripheral palisading (top middle panel) as well as trabecular growth patterns (top right panel). Middle left, middle center, middle right, and bottom left panels show the immunohistochemical expression patterns of *ASCL1*, chromogranin A, synaptophysin, and *YAP1* of xenograft tumors of the VMRC-LCD cell line, respectively, in a high-power view field (×400). *ASCL1* was diffusely positive, chromogranin A and synaptophysin were partially positive, and *YAP1* was completely negative.

antibody in a tumor was defined as positive when more than 0% were stained, and negative when the tumor cells showed complete negative staining.

Generation of *YAP1*-deficient cell lines. In order to achieve the stable knockdown of the *YAP1* gene, SCLC cell lines (SBC3, SBC5, and LCMA) were infected on 12-well plates with lentiviral particles expressing three distinct target-specific shRNA or non-targeting shRNA (sc-38637-V and sc-108080)

(Santa Cruz Biotechnology, Dallas, TX, USA) in the presence of 5 μg/mL polybrene (Santa Cruz Biotechnology). Stably infected cells were selected with 2 μg/mL puromycin for 2 days and 4 μg/mL puromycin for an additional 2 days.

Evaluation of transcriptional activity of *YAP1* by luciferase assay. A PGLIII/TEAD2-Luciferase plasmid was constructed by inserting four tandem repeat sequences containing a TEAD-binding GTTIC (GGAATG) site and its flanking sequences into

Table 4. Positivity for YAP1 in each histological subtype of lung cancer using tissue microarray sections

Histology	YAP1-positive	YAP1-negative	Total
SCLC	1	5	6
LCNEC	3	3	6
NSCLC, except for LCNEC	183	6	189
Total	187	14	201

Small-cell lung cancer (SCLC) versus non-small-cell lung cancer (NSCLC), except for large-cell neuroendocrine carcinoma (LCNEC), $P < 0.0001$ (Fisher's exact test). LCNEC versus NSCLC, except for LCNEC, $P = 0.0013$ (Fisher's exact test).

Table 5. Comparison of YAP1 expression levels with histological subtypes and expression levels of neuroendocrine markers using whole sections of high-grade neuroendocrine tumors

Histology	YAP1 expression		P-value
	Positive	Negative	
SCLC	1	40	<u><0.0001</u>
LCNEC	12	18	
Synaptophysin			
Positive	0	28	<u>0.0010</u>
Negative	13	30	
Chromogranin A			
Positive	0	24	<u>0.0030</u>
Negative	13	34	
ASCL1			
Positive	5	42	<u>0.0264</u>
Negative	8	16	
NCAM			
Positive	7	38	0.5280
Negative	6	20	

LCNEC, large-cell neuroendocrine carcinoma; SCLC, small-cell lung cancer. Underlined P-values are considered significant ($P < 0.05$).

an *XhoI-EcoRI* site upstream of a firefly luciferase reporter gene in a pGL3-Basic Vector (Promega, Fitchburg, WI, USA). A luciferase assay was undertaken in order to monitor the transcriptional activity of YAP1 using the PGLIII/TEAD2-Luciferase plasmid and the Renilla luciferase plasmid pRL-TK as an internal control.

Drug sensitivity. The SBC3, SBC5, LCMA, N417, H146, Lu139, Lu130, H69, H889, H510A, the SBC3-shControl cell lines, SBC3-shYAP1 cell line, SBC5-shControl cell line, SBC5-shYAP1 cell line, LCMA-shControl cell line, and LCMA-shYAP1 cell line were used in triplicate. Cells (1×10^4 cells) were plated on the wells of 96-well microtiter plates. After 24 h, cisplatin was added to the wells at the following final concentrations: 10, 3.3, 1, and 0.1 μM . The cells were then incubated for another 3 days at 37°C. Cells were removed by treatment with trypsin/EDTA solutions, and then counted using the Countess automated cell counter (Invitrogen, Waltham, MA, USA). Results were plotted as cell viability versus \log_{10} (concentration of reagents) and the IC_{50} value was calculated using the software GraphPad Prism 5 (GraphPad Software, San Diego, CA, USA).

Bioinformatic analyses. We used the CLUSTER program (<http://rana.lbl.gov/EisenSoftware.htm>, accessed March 19, 2008) for a cluster analysis of the gene expression data of cell lines. In brief, we carried out average linkage hierarchical clustering of

the 15 cell lines using the mean centering and normalization of genes. We then displayed the results obtained with the aid of TreeView software (<http://rana.lbl.gov/EisenSoftware.htm>, accessed March 21, 2008). The image used a color code to represent relative expression levels. Red represents expression levels greater than the mean for a given gene across all samples. Green represents expression levels less than the mean across samples.

Statistical analysis. Fisher's exact test was used to evaluate clinicopathological relationships. Calculations were carried out with StatView (Abacus Concepts, Berkeley, CA, USA). P-values less than 0.05 were considered significant. Survival curves were generated using the Kaplan–Meier method and differences in survival were analyzed by the Wilcoxon method.

Results

Hierarchical cluster analysis of cell lines derived from high-grade neuroendocrine tumors. We undertook a hierarchical cluster analysis of the 15 high-grade neuroendocrine tumor cell lines (14 SCLC cell lines and H460 cell line) based on the gene expression of Hippo pathway-correlated molecules and neuroendocrine differentiation-correlated molecules containing neuroendocrine markers and myc family genes (gene data shown in Table S1). The results obtained are shown in Figure 1(a). Fifteen cell lines were divided into two distinctive groups: the YAP1-negative floating cell type ($n = 11$) and the YAP1-positive adherent cell type ($n = 4$) (Fig. 1a). The YAP1-negative floating cell type also showed loss of expression of the *WTIP*, *LATS2*, and *JUB* genes (*AJUBA*), which are regulators of YAP1 activity, as well as the loss of the gene expression of *TEAD2*, a transcriptional factor that interacts with YAP1. The expression of *WWTR1* (*TAZ*), a YAP1 paralogue, was also lost in all of the YAP1-negative floating cell types, however, SBC5, one of the YAP1-positive adherent cell types, also showed loss of expression of *WWTR1*. The cell lines showing strong gene expression of neuroendocrine markers belonged to the YAP1-negative floating cell type, whereas all of the cell lines in the YAP1-positive adherent cell type showed weak gene expression of neuroendocrine markers (Fig. 1a,b). We then compared the protein expression level of YAP1 and neuroendocrine markers (chromogranin A, synaptophysin, and NCAM1) among the 15 cell lines tested by Western blotting, and also carried out immunohistochemistry for YAP1 and neuroendocrine markers (chromogranin A, synaptophysin, NCAM1, and ASCL1), using the xenograft tumors of 8 of the 15 cell lines. The results of the Western blot analysis and immunohistochemistry are shown in Figure 2 and Table 3, respectively. We confirmed that cell lines with the loss of YAP1 were positive for neuroendocrine markers, whereas YAP1-positive cell lines were negative for neuroendocrine markers at the protein level. The typical expression patterns of the neuroendocrine markers of the YAP1-positive SCLC cell line SBC5 and YAP1-negative SCLC cell line H69 are shown in Figure 1(c). These results suggest that the loss of YAP1 correlates with the expression of neuroendocrine markers or the floating phenotype. Our immunohistochemical analysis of the xenograft tumors also revealed that it was difficult to determine whether H460 was an LCNEC cell line, because H460 was negative for all of the neuroendocrine markers.

Expression pattern of YAP1 in NSCLC cell lines. We extracted and compared the gene expression of *YAP1*, *WWTR1*, *LATS2*, *WTIP*, *TEAD2*, and neuroendocrine markers from the DNA

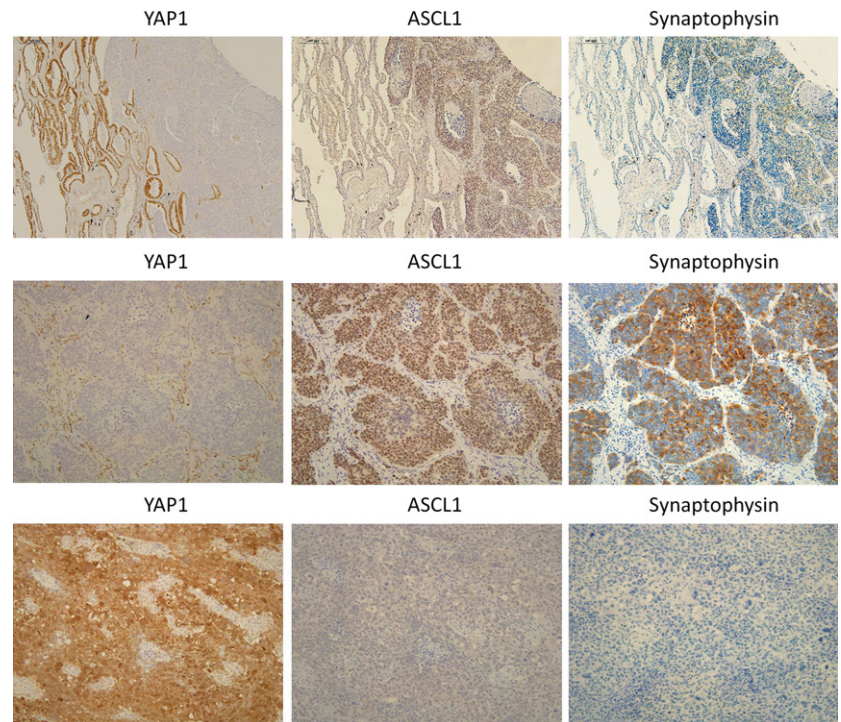


Fig. 4. Top row: panels show YAP1 (left panel), ASCL1 (center panel), and synaptophysin (right panel) stained sections of combined small-cell lung cancer with adenocarcinoma components using serial sections ($\times 100$). Adenocarcinoma components (left) were positive for YAP1 and negative for ASCL1 and synaptophysin, whereas small-cell lung cancer components (right) were negative for YAP1 and positive for ASCL1 and synaptophysin. Middle and bottom panels: YAP1 (left), ASCL1 (center), and synaptophysin (right) stained sections of YAP1-negative and YAP1-positive large cell neuroendocrine carcinoma (LCNEC) cases, respectively, using serial sections ($\times 200$). The YAP1-negative LCNEC case was positive for ASCL1 and synaptophysin (middle panels), whereas the YAP1-positive LCNEC case was negative for ASCL1 and synaptophysin (bottom panels).

array data of 41 NSCLC cell lines including H460, as described in our previous studies.^(21–23) Gene expression data is shown in Table S2. All NSCLC cell lines were positive for *YAP1*, except for VMRC-LCD (Fig. 3a). VMRC-LCD was not a floating cell line, but an adherent cell line established as a primary lung adenocarcinoma cell line. However, VMRC-LCD showed the strongest gene expression of *ASCL1*, *SYP*, and *CHGA* among the 41 NSCLC cell lines examined (Fig. 3a). VMRC-LCD showed the loss of YAP1 and stronger expression of neuroendocrine markers at the protein level than NSCLC cell lines in the Western blot analysis (Fig. 2). In xenograft tumors, histologically, VMRC-LCD cells were found to proliferate to form solid nests with extensive necrosis in the low-power view field (Fig. 3b). In the high-power view field, VMRC-LCD cells, having large nuclei with prominent nucleoli and a more abundant cytoplasm than SCLC, showed solid growth patterns with peripheral palisading (Fig. 3b). Although these tumors sometimes showed trabecular growth patterns (Fig. 2d), no mucin was detected by Alcian blue staining (not shown). VMRC-LCD cells showed high mitotic activity; more than 100 mitotic figures per 10 high-power fields ($\times 400$). The results of the immunohistochemical analysis revealed that VMRC-LCD cells were completely negative for YAP1, diffusely positive for ASCL1, and also partially positive for chromogranin A and synaptophysin (Fig. 3b, Table 3). We examined xenograft tumors under an electron microscope, and found dense-core granules in VMRC-LCD cells (Fig. S1). Based on these results, we concluded that VMRC-LCD was an LCNEC cell line, and that the loss of YAP1 correlated with neuroendocrine features, but not with the floating phenotype. The loss of *WWTR1*, *LATS2*, and *JUB* was also only observed in VMRC-LCD cells, whereas the loss of *WTIP* or *TEAD2* was sometimes observed among the other NSCLC cell lines tested (Table S2).

Expression pattern of YAP1 in TMA sections of primary lung tumors. We carried out immunohistochemistry for YAP1 using TMA sections of 201 primary lung cancers (142

adenocarcinomas, 40 squamous cell carcinomas, 7 pleomorphic carcinomas, 6 SCLCs, and 6 LCNECs). The results obtained are shown in Table 4. The loss of YAP1 was rarer in NSCLCs, except for LCNECs (6/189, 3%), than in SCLCs (5/6, 83%) and LCNECs (3/6, 50%).

Expression patterns of YAP1 and neuroendocrine markers in whole sections of high-grade neuroendocrine lung tumors. We collected whole sections of high-grade neuroendocrine lung tumors (41 SCLCs and 30 LCNECs), and carried out immunohistochemistry for YAP1 and neuroendocrine markers. The results obtained are shown in Table 5. Most SCLCs (40/41, 98%) were completely negative for YAP1, except for one case that was combined SCLC with squamous cell carcinoma components. Eighteen of 30 LCNECs (60%) were also completely negative for YAP1, whereas 12 LCNECs showed strong positivity for YAP1. The loss of YAP1 was significantly more frequent in SCLCs than in LCNECs ($P < 0.0001$) (Table 5). Combined SCLC/LCNEC with adenocarcinoma or squamous cell carcinoma components frequently showed the loss of YAP1 in the components of SCLC/LCNEC, and strong positivity in adenocarcinoma or squamous cell carcinoma components. Among high-grade neuroendocrine lung tumors, the expression of YAP1 inversely correlated with that of synaptophysin, chromogranin A, and ASCL1 ($P = 0.0010$, 0.0030 , and 0.0264 , respectively), and there were also no positive cases for synaptophysin or chromogranin A among YAP1-positive cases (Table 5). Figure 4 shows the typical expression patterns of YAP1 and neuroendocrine markers of combined SCLC with adenocarcinoma components (top panels), YAP1-negative LCNEC (middle panels), and YAP1-positive LCNEC (bottom panels). We speculated that the loss of YAP1 occurs at a relatively early stage of neuroendocrine differentiation, at least before the expression of synaptophysin and chromogranin A, but after the expression of ASCL1 because 5 out of 13 YAP1-positive cases were positive for ASCL1 (Table 5). The relationships between YAP1 expression and clinicopathological factors are shown in Table 6. No

Table 6. Relationships between YAP1 expression levels and clinicopathological factors in 71 high-grade neuroendocrine tumors

	YAP1 expression		P-value
	Positive	Negative	
Pathological stage†			
Stage I	7	25	>0.9999
Stages II–IV	5	21	
T-stage‡			
T1	5	22	>0.9999
T2, T3, T4	8	35	
Nodal involvement§			
Positive	2	19	0.1817
Negative	10	28	
Lymphatic invasion¶			
Positive	2	31	0.1239
Negative	6	21	
Vessel invasion††			
Positive	7	40	>0.9999
Negative	1	11	
Pleural invasion‡‡			
Positive	10	26	0.0658
Negative	3	30	
Tumor size, cm§§			
<3	7	36	0.5351
≥3	6	20	
Pulmonary metastasis¶¶			
Positive	1	3	0.5751
Negative	12	53	
Age, years			
<60	1	8	>0.9999
≥60	12	50	
Sex			
Male	9	55	<u>0.0183</u>
Female	4	3	

†Stages (I or II–IV) of 13 cases were unknown. ‡Pathological T-stage of one case was unknown. §Presence or absence of nodal involvement in 12 cases was unknown. ¶Presence or absence of lymphatic invasion in 11 cases was unknown. ††Presence or absence of vessel invasion in 11 cases was unknown. ‡‡Presence or absence of pleural invasion in two cases was unknown. §§Tumor sizes of two cases were unknown. ¶¶Presence or absence of pulmonary metastasis in two cases was unknown. Underlined P-values are considered significant ($P < 0.05$).

clinicopathological factor correlated with the expression of YAP1, except for sex.

Recently, Hamanaka *et al.*⁽²⁵⁾ reported that SCLC cases with low neuroendocrine marker expression showed good prognosis. In our study, some YAP1-negative SCLC cases were also negative for chromogranin A, synaptophysin, and NCAM1, and the survival analysis revealed that neuroendocrine marker-negative cases showed much better prognosis than neuroendocrine marker-positive cases among YAP1-negative cases (Fig. S2).

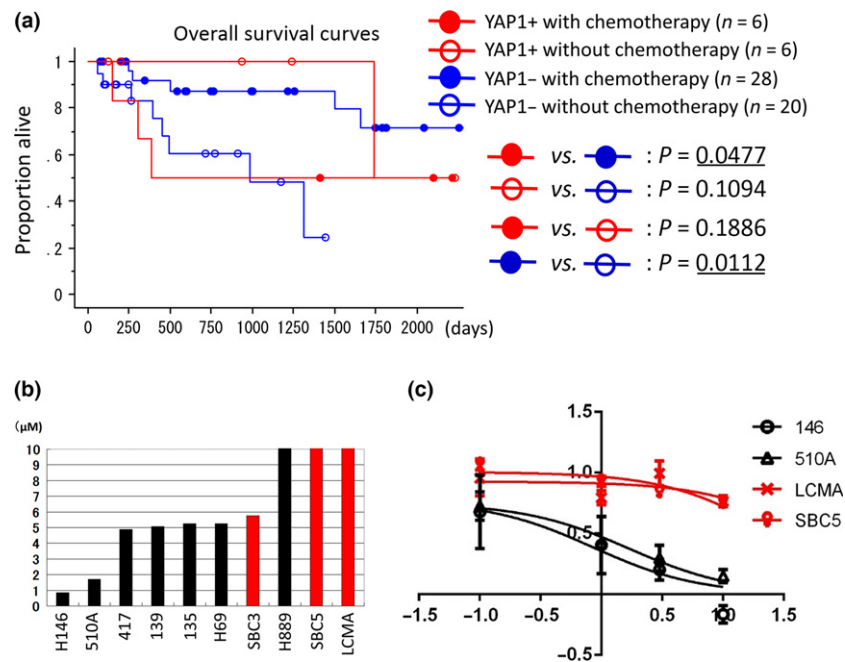
Loss of YAP1 correlated with chemosensitivity in high-grade neuroendocrine tumors. Figure 5(a) shows the results of the survival analysis of 60 high-grade neuroendocrine tumor cases without neoadjuvant chemotherapy. Cases with adjuvant chemotherapy ($n = 34$) had slightly better prognoses than those without ($n = 26$, $P = 0.1559$). However, among YAP1-negative cases ($n = 48$), cases with adjuvant chemotherapy ($n = 28$) showed significantly better prognoses than those without ($n = 20$, $P = 0.0112$) (Fig. 5a). Among cases with

adjuvant chemotherapy ($n = 34$), YAP1-negative cases ($n = 28$) showed significantly better prognoses than YAP1-positive cases ($n = 6$, $P = 0.0477$) (Fig. 5a), whereas, among cases without adjuvant chemotherapy ($n = 26$), YAP1-negative cases ($n = 20$) showed slightly worse prognoses than YAP1-positive cases ($n = 6$, $P = 0.1094$) (Fig. 5a). These results suggest that, among high-grade neuroendocrine tumors, YAP1-negative cases were more chemosensitive than YAP1-positive cases.

Positivity for YAP1 correlated with resistance to cisplatin in 10 SCLC cell lines. We examined sensitivity to cisplatin in a panel of 10 SCLC cell lines classified into the YAP1-negative group ($n = 7$) and YAP1-positive group ($n = 3$). In a comparison of IC_{50} values for cisplatin between the YAP1-positive and YAP1-negative groups, we found that YAP1-positive group cell lines were significantly more resistant to cisplatin than YAP1-negative group cell lines ($P = 0.0304$, Mann–Whitney *U*-test) (Fig. 5b). Figure 5(c) shows the dose–response curves of two YAP1-negative cell lines (H146 and H510A) and two YAP1-positive cell lines (SBC5 and LCMA).

Knockdown of YAP1 induces neuroendocrine marker RAB3A. In order to investigate the effects of the loss of function of YAP1, YAP1-positive SCLC cell lines (SBC3, SBC5, and LCMA) were infected with lentiviral shYAP1 and shControl. We confirmed that the protein expression level and transcriptional activity of YAP1 were reduced more by shYAP1 than by shControl with Western blotting and luciferase assay, respectively (Fig. 6a,b). We examined sensitivity to cisplatin using SBC3-, SBC5-, and LCMA-shControl and shYAP1 cell lines in order to investigate the impact of YAP1 on drug sensitivity; however, reductions in the expression of YAP1 did not improve sensitivity to cisplatin in SBC3, SBC5, or LCMA (Fig. 6c). We then undertook a gene expression analysis by mRNA-Seq using the SBC3-, SBC5-, and LCMA-shControl and shYAP1 cell lines, extracted genes with signals greater than or equal to 1 (gene data shown in Table S3), and selected genes upregulated or downregulated by shYAP1 among all three YAP1-positive SCLC cell lines (SBC3, SBC5, and LCMA). Table 7 shows the top 20 genes upregulated or downregulated by shYAP1 depending on the average quotient of shYAP1/shControl. We carried out a cluster analysis of the 15 high-grade neuroendocrine tumor cell lines using the genes listed in Table 7, except for the *YAP1* gene. The cell lines were clearly classified into a neuroendocrine marker-positive group ($n = 11$) and neuroendocrine marker-negative group ($n = 4$) (Table S4, Fig. S3). These results suggest that the downregulation of YAP1 affects the genes characterizing the neuroendocrine phenotype. We extracted the genes selectively expressed as the neuroendocrine marker-positive group or neuroendocrine marker-negative group (NE+ group/NE– group >3 or $1 < 3$) showing positive or negative correlations with the expression of *YAP1* (correlation co-efficient >0.3 or <-0.3). The results obtained are shown in Table 8. We found that *RAB3A* was upregulated by shYAP1. *RAB3A* is a synaptic vesicle-specific protein, similar to synaptophysin, is specifically expressed in normal neuroendocrine cells and malignant neuroendocrine tumors, and was previously reported to be a useful neuroendocrine marker.⁽²⁶⁾ In this report, we did not show the immunohistochemical expression pattern of *RAB3A* in high-grade neuroendocrine tumor cases, but instead we confirmed by Western blotting that *RAB3A* was strongly expressed in YAP1-negative cell lines with high expression levels of neuroendocrine markers (Fig. 2). We speculated that the loss of YAP1 is involved in the neuroendocrine differentiation of lung

Fig. 5. (a) Patient survival according to YAP1 expression levels. Patients were separated into the following four groups: YAP1-positive cases with adjuvant chemotherapy (YAP1+ with chemotherapy), YAP1-positive cases without adjuvant chemotherapy (YAP1+ without chemotherapy), YAP1-negative cases with adjuvant chemotherapy (YAP1- with chemotherapy), and YAP1-negative cases without adjuvant chemotherapy (YAP1- without chemotherapy). Underlined *P*-values are considered significant ($P < 0.05$). (b) Comparisons of IC_{50} values for cisplatin. The upper-limit values of graphs are set to be $10 \mu\text{mol/L}$. Red bars indicate YAP1-positive cell lines; black bars indicate YAP1-negative cell lines. (c) Dose-response curves of four cell lines: H146, H510A, LCMA, and SBC5. H146 and H510A (black lines) were YAP1-negative small-cell lung cancer cell lines, and LCMA and SBC5 (red lines) were YAP1-positive small-cell lung cancer cell lines. The x-axis indicates the \log_{10} (concentration of cisplatin) and the y-axis indicates cell viability = (mean absorbance in test wells)/(mean absorbance in control wells). H146 and H510A were sensitive to cisplatin ($IC_{50} = 0.8573$ and 1.698 , respectively), while LCMA and SBC5 were resistant ($IC_{50} = 58.69$ and 25.48 , respectively).



tumors through the upregulation of RAB3A. We noted that ShYAP1 also downregulated the expression of *AMTOL2*, *JUB* (*AJUBA*), and *WTIP*, which are regulators of YAP1. Using the antibodies available for Western blotting, we confirmed that the protein expression levels of *AJUBA* and *AMOTL2* were downregulated by shYAP1 (Fig. 6d). This may have been caused by a negative-feedback mechanism. We also confirmed that the expression of *AJUBA* was completely lost in the YAP1-negative cell lines strongly expressing neuroendocrine markers (Fig. 2).

Discussion

In the present study, we revealed that the loss of YAP1 correlated with the strong expression of neuroendocrine markers, and the knockdown of YAP1 induced the expression of the neuroendocrine marker *RAB3A*, suggesting the possible involvement of YAP1 in the regulation of neuroendocrine differentiation. We also showed that the loss of YAP1 is a promising predictor of chemotherapy responses in SCLC and LCNEC cases using a panel of high-grade neuroendocrine tumor cell lines and sections.

Yes-associated protein 1 functions as an oncogene; its overexpression overcomes cell contact inhibition, induces epithelial-mesenchymal transition, and promotes cancer cell proliferation and invasion.^(12–14) The strong expression of YAP1 has frequently been observed in various tumors, such as hepatocellular carcinoma, ovarian cancer, and NSCLC,^(12–16) and its overexpression in NSCLC has been correlated with a poor prognosis.⁽¹⁴⁾ However, in terms of SCLC, only a few studies have reported the tumor-suppressive function of YAP1, inducing apoptosis in combination with p73.^(17,18) Wu *et al.*⁽¹⁷⁾ reported that some single nucleotide polymorphisms within the promoter region of YAP1 were associated with the downregulation of the gene and survival of SCLC patients. Nishikawa *et al.*⁽¹⁸⁾ found that the downregulation of YAP1 by ASCL1 through the activation of mir375 inhibited apoptosis. However, no studies have focused on the role of YAP1 in neuroendocrine differentiation until now. Our analysis of 15 high-grade neuroendocrine tumor

cell lines and 41 NSCLC cell lines showed the loss of YAP1 in all cell lines strongly expressing neuroendocrine markers. Our immunohistochemical analysis of 71 high-grade neuroendocrine tumors also revealed an inverse correlation between YAP1 and neuroendocrine markers, and also that the number of YAP1-positive and neuroendocrine marker-positive cases is more limited than negative cases. We also showed that the knockdown of YAP1 induced the neuroendocrine marker, the *RAB3A* gene. *RAB3A* is a synaptic vesicle-specific protein, specifically expressed in normal neuroendocrine cells and malignant neuroendocrine tumors. These results suggest that YAP1 is involved in the repression of neuroendocrine differentiation. In this study, we did not stain carcinoid tumors for YAP1, but could confirm that carcinoid tumors were completely negative for YAP1 in the human protein atlas database (<http://www.proteinatlas.org/>), which suggested that loss of YAP1 was not specific to high-grade neuroendocrine tumors, but common in neuroendocrine tumors.

Unlike the cell lines, there were 5 YAP1-positive and ASCL1-positive cases among 71 cases, which suggested that loss of YAP1 would occur after ASCL1 expression. It would be consistent with the report that ASCL1 induced suppression of YAP1 through mir375 in SCLC.⁽¹⁷⁾ However, 16 YAP1-negative and ASCL1-negative cases were also found among 71 cases, which suggested that, although some high-grade neuroendocrine tumors would lose ASCL1 expressions in the progression, the expressions of YAP1 would not be recovered. ASCL1-induced suppression through miRNA could not efficiently explain the complete loss of YAP1 in high-grade neuroendocrine tumors. We were suspicious of the involvement of DNA methylation, but DNA methylation inhibitor, 5-aza-2-deoxycytidine treatment did not upregulate *YAP1* gene expression in YAP1-negative SCLC cell lines (data not shown). We also could find no specific genetic abnormalities in the *YAP1* gene in YAP1-negative SCLC cell lines by mRNA-Seq. We need to study further to find the mechanism that causes the loss of YAP1.

Our survival analysis of 71 high-grade neuroendocrine tumors revealed that YAP1 is a useful marker for stratifying

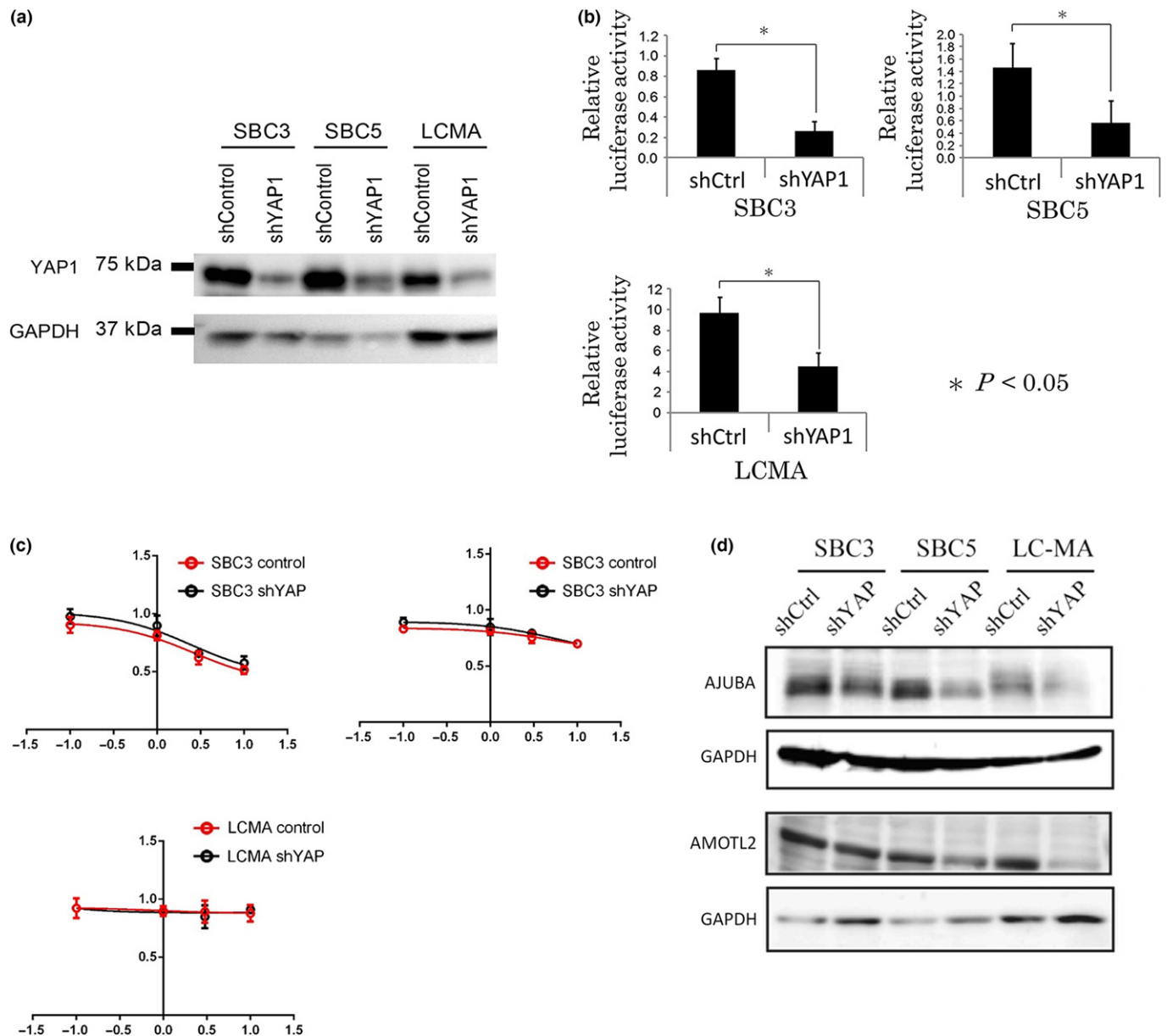


Fig. 6. (a) SBC3, SBC5, and LCMA cell lines were infected with a lentivirus encoding the indicated shYAP1 or the control. Drug-selected cells were examined for the expression of YAP1 and GAPDH by immunoblotting. (b) Luciferase assay to monitor the transcriptional activity of YAP1 using a PGLIII/TEAD2-Luciferase plasmid and the Renilla luciferase plasmid pRL-TK as an internal control. The transcriptional activity of YAP1 was downregulated more by shYAP1 than by shControl. (c) Dose-response curves of SBC3, SBC5, and LCMA cell lines infected with a lentivirus encoding the indicated shYAP1 (black line) or control (red line). The x-axis indicates the \log_{10} (concentration of cisplatin), and the y-axis indicates cell viability = (mean absorbance in test wells)/(mean absorbance in control wells). (d) Western blot analysis of protein expression levels of AMOTL2 and AJUBA using SBC3-shControl, SBC3-shYAP1, SBC5-shControl, SBC5-shYAP1, LCMA-shControl, and LCMA-shYAP1 cell lines.

high-grade neuroendocrine tumors into chemosensitive and chemoresistant groups. Our survival curves in Figure 5(a) also showed that, among YAP1-positive cases, the adjuvant chemotherapy group had a slightly worse prognosis than the non-adjuvant chemotherapy group, which suggested that adverse drug reactions may exceed the beneficial effects of platinum-based chemotherapy in YAP1-positive high-grade neuroendocrine tumors. Recently, YAP1 has been attracting attention as a key molecule to determine the resistance of various tumors to platinum, including NSCLC, oral cancer, cervical cancer, thyroid cancer, and ovarian cancer.^(27–30) Cheng *et al.*⁽²⁶⁾ showed that the downregulation of YAP1 by

verteporfin (a YAP1 inhibitor) sensitized cells to DNA-damaging agents.

In the present study, the knockdown of YAP1 by shYAP1 did not induce sensitivity to cisplatin, and also did not induce neuroendocrine markers other than the *RAB3A* gene in YAP1-positive SCLC cell lines. These results suggest that the knockdown of YAP1 is necessary, but not sufficient for inducing neuroendocrine differentiation. *WWTR1* (*TAZ*), YAP1 homologue, was also lost in neuroendocrine marker-positive cell lines. Interestingly, the expression levels of *STMN2* (*SCG10*), one of the regulators of neuroendocrine secretion,⁽³¹⁾ increased more than 3-fold only in SBC5, the YAP1-positive and

Table 7. Top 20 genes upregulated or downregulated by shYAP1 in YAP1-positive small-cell lung cancer cell lines LCMA, SBC3, and SBC5

Upregulated genes		Downregulated genes	
Genes	shYAP1/shControl	Genes	shYAP1/shControl
<i>FOS</i>	1.772226	<i>YAP1</i>	0.271919
<i>EGR1</i>	1.537839	<i>MYL9</i>	0.521909
<i>C11orf71</i>	1.504796	<i>NPIP</i>	0.534952
<i>RCC1</i>	1.411171	<i>AMOTL2</i>	0.565497
<i>RAB3A</i>	1.399324	<i>SORL1</i>	0.57968
<i>MLLT11</i>	1.390264	<i>MEGF6</i>	0.581002
<i>ID1</i>	1.389716	<i>WTIP</i>	0.613103
<i>C1orf53</i>	1.389643	<i>LRP1</i>	0.621807
<i>TUBB3</i>	1.377206	<i>CLU</i>	0.629044
<i>SMAD9</i>	1.374954	<i>SYNE2</i>	0.639216
<i>METTL12</i>	1.354466	<i>FAHD2B</i>	0.650478
<i>ELL3</i>	1.333245	<i>MAFF</i>	0.654306
<i>HMGC51</i>	1.328731	<i>RND3</i>	0.658228
<i>SNORD17</i>	1.328284	<i>CADM4</i>	0.660109
<i>ID1</i>	1.323846	<i>FAM131C</i>	0.660935
<i>GLYCTK</i>	1.32376	<i>JMJD7-PLA2G4B</i>	0.66569
<i>TNFAIP8</i>	1.315202	<i>JUB</i>	0.668008
<i>INSIG1</i>	1.311661	<i>VLDLR</i>	0.668359
<i>LDHA</i>	1.306133	<i>PPP1R15A</i>	0.670045
<i>PTRH1</i>	1.291859	<i>RHBDF1</i>	0.671982

Table 8. Genes selectively expressed in neuroendocrine marker-positive ($n = 11$) or neuroendocrine marker-negative ($n = 4$) (NE+ group/NE- group >3 or $<1/3$) lung cancer cell lines, showing positive or negative correlations with the expression of YAP1 (correlation coefficient [Correl] >0.3 or <-0.3)

Upregulated genes			Downregulated genes		
Genes	NE+/NE-	Correl	Genes	NE+/NE-	Correl
<i>RAB3A</i>	20.94204	-0.60259	<i>YAP1</i>	0.016573	1.000000
<i>SMAD9</i>	5.662386	-0.56706	<i>WTIP</i>	0.064979	0.870644
<i>HMGC51</i>	4.311002	-0.34515	<i>MYL9</i>	0.016699	0.816232
<i>TUBB3</i>	3.536579	-0.33223	<i>LRP1</i>	0.297128	0.765227
			<i>RHBDF1</i>	0.133056	0.721056
			<i>JUB</i>	0.062124	0.650110
			<i>AMOTL2</i>	0.051046	0.613924
			<i>RND3</i>	0.190660	0.434551

Genes shown in bold, NE+ group/NE- group >10 or $<1/10$, Correl >0.6 or <-0.6 . Selected genes are among the top 20 upregulated or downregulated by shYAP1 in YAP1-positive small-cell lung cancer cell lines LCMA, SBC3, and SBC5.

WWTR1-negative SCLC cell line, by shYAP1 treatment, and high-level expressions of *STMN2* were characteristically shown in neuroendocrine marker-positive SCLC cell lines (data not

shown). These results suggested that suppression of both of YAP1 and WWTR1 might be important for inducing neuroendocrine differentiation. We did not focus on TEAD2 in this report, but the cell lines with high level expressions of neuroendocrine markers characteristically showed complete loss of *TEAD2* gene expression. TEAD2 is transcription factor correlated with neuronal development.⁽³²⁾ We need to elucidate each role of YAP-TEAD1-4 or WWTR1-TEAD1-4 complex-mediated transcription, to reveal the meaning of loss of WWTR1 and TEAD2 in SCLC; this will be the focus of our future study.

Recently, YAP1 has been reported to inhibit the squamous differentiation of LKB1-deficient lung adenocarcinomas.⁽³³⁾ YAP1 must be a key regulator of differentiation, and searching for genetic changes in addition to the loss of YAP1 that induce neuroendocrine differentiation will help to elucidate its mechanism of action.

In summary, the loss of YAP1 may define a unique subset of high-grade neuroendocrine tumors. These tumors strongly express neuroendocrine markers and show chemosensitivity.

Acknowledgments

This study was supported in part by the Japan Society for the Promotion of Science (KAKENHI grant nos. 16K08672, 90198424, 25460432, and 30182108), Grants for Research on Human Genome Tailor-made from the Ministry of Health, Labor, and Welfare of Japan, the Smoking Research Foundation, and the Foundation for the Development of the Community.

Disclosure Statement

Matsubara Daisuke supported by the Smoking Research Foundation.

Abbreviations

AMOTL2	angiomin-like 2
ASCL1	Achaete-scute homolog 1
CAV	cyclophosphamide + doxorubicin + vincristine
CBDCA	carboplatin
CDDP	cisplatin
CPT11	irinotecan
GEM	gemcitabine
LATS1/2	large tumor suppressor 1/2
LCNEC	large-cell neuroendocrine carcinoma
mir	miRNA
mRNA-Seq	mRNA sequencing
NCAM	neural cell adhesion molecule
NSCLC	non-small-cell lung cancer
SCLC	small-cell lung cancer
TEAD2	TEA domain transcription factor 2
TMA	tissue microarray
VNR	vinorelbine
VP16	etoposide
WWTR1	WW domain containing transcription regulator 1
YAP1	yes-associated protein 1

References

- Travis WD, Brambilla E, Burke AP *et al.* *WHO Classification of Tumours of the Lung, Pleura, Thymus and Heart*, 4th edn. Lyon, France: IARC, 2015.
- Sundström S, Bremnes RM, Kaasa S *et al.* Cisplatin and etoposide regimen is superior to cyclophosphamide, epirubicin, and vincristine regimen in small-cell lung cancer: results from a randomized phase III trial with 5 years' follow-up. *J Clin Oncol* 2002; **20**: 4665–72.

- Travis WD. Advances in neuroendocrine lung tumors. *Ann Oncol* 2010; **21** (Suppl 7): vii65–71.
- Igawa S, Watanabe R, Ito I *et al.* Comparison of chemotherapy for unresectable pulmonary high-grade non-small cell neuroendocrine carcinoma and small-cell lung cancer. *Lung Cancer* 2010; **68**: 438–45.
- Iyoda A, Hiroshima K, Moriya Y *et al.* Prospective study of adjuvant chemotherapy for pulmonary large cell neuroendocrine carcinoma. *Ann Thorac Surg* 2006; **82**: 1802–7.

- 6 Yamazaki S, Sekine I, Matsuno Y *et al.* Clinical responses of large cell neuroendocrine carcinoma of the lung to cisplatin-based chemotherapy. *Lung Cancer* 2005; **49**: 217–23.
- 7 Rossi G, Cavazza A, Marchioni A *et al.* Role of chemotherapy and the receptor tyrosine kinases KIT, PDGFR α , PDGFR β , and met in large-cell neuroendocrine carcinoma of the lung. *J Clin Oncol* 2005; **23**: 8774–85.
- 8 Harvey KF, Zhang X, Thomas DM. The Hippo pathway and human cancer. *Nat Rev Cancer* 2013; **13**: 246–57.
- 9 Zhao B, Wei X, Li W *et al.* Inactivation of YAP oncoprotein by the Hippo pathway is involved in cell contact inhibition and tissue growth control. *Genes Dev* 2007; **21**: 2747–61.
- 10 Zhao B, Lei QY, Guan KL. The Hippo-YAP pathway: new connections between regulation of organ size and cancer. *Curr Opin Cell Biol* 2008; **20**: 638–46.
- 11 Zhao B, Tumaneng K, Guan KL. The Hippo pathway in organ size control, tissue regeneration and stem cell self-renewal. *Nat Cell Biol* 2011; **13**: 877–83.
- 12 Zender L, Spector MS, Xue W *et al.* Identification and validation of oncogenes in liver cancer using an integrative oncogenomic approach. *Cell* 2006; **125**: 1253–67.
- 13 Overholtzer M, Zhang J, Smolen GA *et al.* Transforming properties of YAP, a candidate oncogene on the chromosome 11q22 amplicon. *Proc Natl Acad Sci USA* 2006; **103**: 12405–10.
- 14 Wang Y, Dong Q, Zhang Q *et al.* Overexpression of yes-associated protein contributes to progression and poor prognosis of non-small-cell lung cancer. *Cancer Sci* 2010; **101**: 1279–85.
- 15 Xu MZ, Yao TJ, Lee NP *et al.* Yes-associated protein is an independent prognostic marker in hepatocellular carcinoma. *Cancer* 2009; **115**: 4576–85.
- 16 Hall CA, Wang R, Miao J *et al.* Hippo pathway effector Yap is an ovarian cancer oncogene. *Cancer Res* 2010; **70**: 8517–25.
- 17 Wu C, Xu B, Yuan P *et al.* Genome-wide interrogation identified YAP1 variants associated with survival of small-cell lung cancer patients. *Cancer Res* 2010; **70**: 9721–9.
- 18 Nishikawa E, Osada H, Okazaki Y *et al.* miR-375 is activated by ASH1 and inhibits YAP1 in a lineage dependent manner in lung cancer. *Cancer Res* 2011; **71**: 6165–73.
- 19 Tatematsu T, Sasaki H, Shimizu S *et al.* Investigation of neurotrophic tyrosine kinase receptor 1 fusions and neurotrophic tyrosine kinase receptor family expression in non-small-cell lung cancer and sensitivity to AZD7451 in vitro. *Mol Clin Oncol* 2014; **2**: 725–30.
- 20 Lee M, Draoui M, Zia F *et al.* Epidermal growth factor receptor monoclonal antibodies inhibit the growth of lung cancer cell lines. *J Natl Cancer Inst Monogr* 1992; **13**: 117–23.
- 21 Matsubara D, Ishikawa S, Sachiko O *et al.* Co-activation of epidermal growth factor receptor and c-MET defines a distinct subset of lung adenocarcinomas. *Am J Pathol* 2010; **177**: 2191–204.
- 22 Matsubara D, Ishikawa S, Oguni S *et al.* Molecular predictors of sensitivity to the MET inhibitor PHA665752 in lung carcinoma cells. *J Thorac Oncol* 2010; **5**: 1317–24.
- 23 Matsubara D, Kishaba Y, Ishikawa S *et al.* Lung cancer with loss of BRG1/BRM, shows epithelial mesenchymal transition phenotype and distinct histologic and genetic features. *Cancer Sci* 2013; **104**: 266–73.
- 24 Ito T, Williams-Nate Y, Iwai M *et al.* Transcriptional regulation of the CADM1 gene by retinoic acid during the neural differentiation of murine embryonal carcinoma P19 cells. *Genes Cells* 2011; **16**: 791–802.
- 25 Hamanaka W, Motoi N, Ishikawa S *et al.* A subset of small cell lung cancer with low neuroendocrine expression and good prognosis: a comparison study of surgical and inoperable cases with biopsy. *Hum Pathol* 2014; **45**: 1045–56.
- 26 Culine S, Rousseau-Merck MF, Honoré N *et al.* Specific expression of the ras-related rab3A gene in human normal and malignant neuroendocrine cells. *Cancer* 1992; **70**: 2552–6.
- 27 Cheng H, Zhang Z, Rodriguez-Barrueco R *et al.* Functional genomics screen identifies YAP1 as a key determinant to enhance treatment sensitivity in lung cancer cells. *Oncotarget* 2015; **22**: 28977–88. doi: 10.18632/oncotarget.6721.
- 28 Yoshikawa K, Noguchi K, Nakano Y *et al.* The Hippo pathway transcriptional co-activator, YAP, confers resistance to cisplatin in human oral squamous cell carcinoma. *Int J Oncol* 2015; **46**: 2364–70.
- 29 Lorenzetto E, Brenca M, Boeri M *et al.* YAP1 acts as oncogenic target of 11q22 amplification in multiple cancer subtypes. *Oncotarget* 2014; **5**: 2608–21.
- 30 Xia Y, Chang T, Wang Y *et al.* YAP promotes ovarian cancer cell tumorigenesis and is indicative of a poor prognosis for ovarian cancer patients. *PLoS One* 2014; **9**: e91770.
- 31 Mahapatra NR, Taupenot L, Courel M *et al.* The trans-Golgi proteins SCLIP and SCG10 interact with chromogranin A to regulate neuroendocrine secretion. *Biochemistry* 2008; **47**: 7167–78.
- 32 Kaneko KJ, Kohn MJ, Liu C, DePamphilis ML. Transcription factor TEAD2 is involved in neural tube closure. *Genesis* 2007; **45**: 577–87.
- 33 Gao Y, Zhang W, Han X *et al.* YAP inhibits squamous transdifferentiation of Lkb1-deficient lung adenocarcinoma through ZEB2-dependent DNp63 repression. *Nat Commun* 2014; **5**: 4629.

Supporting Information

Additional Supporting Information may be found online in the supporting information tab for this article:

Appendix S1. Materials and methods.

Fig. S1. Electron microscopy of xenograft tumors of VMRC-LCD lung cancer cell line.

Fig. S2. Patient survival of YAP1-negative high-grade neuroendocrine tumor cases, according to neuroendocrine expression levels.

Fig. S3. Hierarchical cluster analysis of 15 high-grade neuroendocrine lung tumor cell lines using genes upregulated or downregulated by shYAP1.

Table S1. Gene expression data of Hippo pathway molecules, neuroendocrine markers, and the myc family in 15 high-grade neuroendocrine tumor cell lines.

Table S2. Gene expression data of Hippo pathway molecules, neuroendocrine markers, and the myc family in 41 non-small-cell lung cancer cell lines.

Table S3. Gene expression analysis data of SBC3-, SBC5-, and LCMA-shControl and shYAP1 cell lines. The genes with signals greater than or equal to 1 are listed.

Table S4. Expression data of genes listed in Table 7 in 15 high-grade neuroendocrine tumor cell lines.